

Chapter 2

Synthetic Hydrogels for Expansion of Functional Endothelial Cells



Yong Mei Chen, Xue Qi Zhao, and Zhen Qi Liu

Abstract Endothelial cells have presented a wide variety of applications including tissue engineering, artificial organs, and pharmaceutical drug screening. The new insight in exploring synthetic hydrogels which are suitable for expansion of endothelial cells and keeping their original functions will open a new era of soft and wet biomaterials as active templates for cell expansion. In this chapter, we introduce a cell culture system based on protein-free synthetic hydrogels for expansion of endothelial cells. The negatively charged synthetic hydrogels, such as PNaAMPS and PNaSS, can promote endothelial cell proliferation to form a monolayer, without surface modification of any cell-adhesive proteins or peptides, under the environment of serum-containing medium. Moreover, the synthetic hydrogels can maintain the original functions of the expanded cells. In the sections of the effect of chemical structure and zeta potential on cell behaviors, we introduce the effect of physicochemical properties of fully synthetic hydrogels, i.e., chemical structure, charge density, and surface topography, on static cell behaviors (adhesion, spreading, morphology, proliferation, cytoskeletal structure, and focal adhesion) and dynamic cell behaviors (migration velocity, morphology oscillation). In addition, the effect of hydrogel properties on cell behaviors is correlated well with the adsorption of protein derived from cell culture medium. In the section of application of protein-free hydrogels in biomedical field, the platelet compatibility and surface friction of endothelial cell monolayers cultured on hydrogel templates, selective cell adhesion and proliferation on micro-patterned hydrogel surfaces, as well as proliferation of endothelial cells on tough hydrogels are introduced.

Y. M. Chen (✉) · X. Q. Zhao · Z. Q. Liu

College of Bioresources Chemical and Materials Engineering, Shaanxi University of Science and Technology, Xi'an 710021, China

State Key Laboratory for Strength and Vibration of Mechanical Structures, International Center for Applied Mechanics and School of Aerospace, School of Science, Collaborative Innovation Center of Suzhou Nano Science and Technology, Xi'an Jiaotong University, Xi'an, China

e-mail: chenym@mail.xjtu.edu.cn

Keywords Synthetic hydrogels · Endothelial cells · Cell expansion · Cell functions

2.1 Introduction

Cell cultivation systems provide immense potential for large-scale cell expansion, meeting the requirements of cellular source in biomedical field, including tissue engineering, drug screening programs, cell therapy, and disease models. For instance, in order to treat the patients with the disease of heart attack, multiple sclerosis, or diabetes, billions of cells for each patient should be prepared in vitro. In native biological tissues, most mammalian cells are anchorage-dependent, that is, for supporting their viability, proliferation, and functionalities, they should adhere to and spread on extracellular matrix (ECM) with a suitable softness and viscoelasticity. It is challenge to develop the ideal templates for cell cultivation systems which have the similar characterizations with ECM and take full advantages of their features. Hydrogel, a kind of viscoelastic biomaterial swelling a large amount of water-based solution in its chemical or physical cross-linked polymer networks, would be ideally suited to meet this challenge. They can provide biomimetic ECM microenvironment for cells including high water content, tissue-like elasticity, and transportation of oxygen, nutrients, and metabolites [1–4].

For expanding different types of cell populations, a diversity culture systems based on various materials should be developed. So far, a diversity of hydrogels including nature macromolecules, proteins, peptides, and synthetic polymers have been explored as templates for cell expansion. Although the number of cell cultivation systems based on nature-derived hydrogels (e.g., Matrigel [5], collagen [6, 7], and fibrin [8]) and protein-modified (e.g., fibronectin [9] and RGD [10]) hydrogels continues to rise, these systems are currently suboptimal. They have some defects, such as batch-to-batch biological variations, xenogenic contaminants, and difficulty in tuning physicochemical properties [11, 12]. Moreover, the hydrogels derived from proteins and peptides are too expensive to be widely used in large-scale cell cultivation systems. The aforementioned limitations can be overcome through the use of fully synthetic hydrogels that offer several advantages: (1) easily fine-tunable and controllable physicochemical properties including chemical structure, Young's modulus, and charge density; (2) good reproducibility, no infection, low cost, and prone to large-scale manufacture; and (3) superb transparency that is convenient for microscopic observation and in situ assessment of the static and dynamic behaviors in the process of cell cultivation [1, 13–15].

We developed a cell culture system based on protein-free full synthetic hydrogels for expansion of various kinds of cells. It is noteworthy that the full synthetic hydrogels mentioned herein are not modified by any cell-adhesive proteins or peptides before cell cultivation. Under the environment of serum-containing medium, the full synthetic hydrogels can support the expansion of various types of cell lineages, including endothelial cells [1, 14, 16–18], rabbit synovial tissue-derived fibroblast cells [16], human articular chondrocytes [19], murine chondrogenic

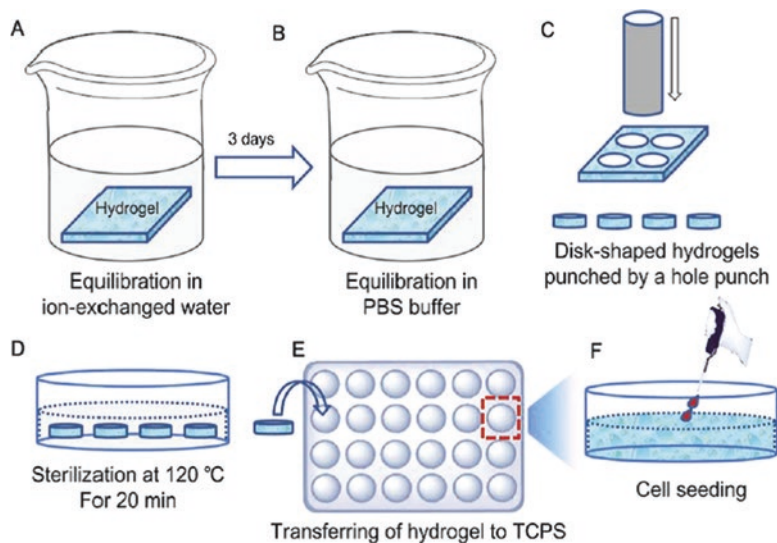
ATDC5 cells [20], retinal pigment epithelium [15], and mouse embryonic stem cells [4]. Especially, the full synthetic hydrogels are not just templates for supporting cell expansion, but they also can manipulate the functions of cells. For example, in the case of endothelial cells, the behaviors of antiplatelet performance, glycocalyx secretion, and low friction are dependent on the properties of hydrogels. In this chapter, we mainly introduce the novel ideas and attractive examples of expansion of endothelial cells via synthetic hydrogel-based culture system. The behaviors of two types of endothelial cells derived from human, i.e., human umbilical vein endothelial cells (HUVECs) and human coronary artery endothelial cells (HCAECs), as well as the endothelial cells from bovine, i.e., bovine fetal aorta endothelial cells (BFAECs), are investigated.

In the *in vivo* vascular systems, functional endothelial cells decorate on the inner surface of blood vessels. Endothelial cell is a kind of special cell that constitutes a monolayer separately circulating blood from the tubular tissues, playing a wide variety of critical physiological functions, for example, thrombosis, hemostasis, angiogenesis, and atherosclerosis. However, blood clot is a major problem of artificial cardiovascular system [14]. For the ideal artificial blood vessels for tissue engineering, they should have the structure similar to biological blood vessels and take full advantages of cell functions. The promising strategy that protects procoagulant activity of artificial blood vascular is the expansion of a functional endothelial cell monolayer on the inner surface of artificial blood vascular. Thus, the artificial cardiovascular system desires the coverage of endothelial cell monolayer on the inner surface of the artificial blood vascular, which can play a lot of functions, especially to inhibit thrombosis [17]. The hydrogels facilitating the expansion of endothelial cells to a cell monolayer are a valuable functional soft biomaterial potentially used for artificial blood vascular.

It is well known that cells easily lose their intrinsic functions after being cultured *in vitro*, so is endothelial cell. Therefore, we should develop hydrogel-based cell cultivation systems that have the advantages of facilitating endothelial cell expansion and forming a continuous monolayer which possesses intrinsic functions of endothelial cells. Our research demonstrated that fully synthetic hydrogels can meet this requirement. Herein, the effect of physicochemical properties of fully synthetic hydrogels, i.e., chemical structure, charge density, and surface topography, on static cell behaviors (adhesion, spreading, morphology, proliferation, cytoskeletal structure, and focal adhesion), dynamic cell behaviors (migration velocity, morphology oscillation), and cell functions (platelet compatibility, surface friction) will be introduced.

2.2 Cell Cultivation on Protein-Free Synthetic Hydrogels

To extend fully synthetic hydrogels in tissue engineering, a basic requirement is the stimulation of cell spreading and proliferation. We established an original cell cultivation system that directly cultured cells on the surface of a series of fully



Scheme 2.1 Schematic representation of cell cultivation processes on the synthetic hydrogels without modification by cell-adhesive proteins or peptides. (a) Sheet-shaped hydrogels are equilibrated in ion-exchanged water. (b) Sheet-shaped hydrogels are equilibrated in PBS. (c) Disk-shaped PBS-equilibrated hydrogels are punched out of the sheet-shaped hydrogels by a hole punch. (d) Disk-shaped PBS-equilibrated hydrogels are sterilized by autoclaving (120 °C, 20 min). (e) The sterilized hydrogels are transferred into 24-well or 6-well TCPS. (f) Cells are directly seeded on pure synthetic hydrogels. (Reprinted with permission from Ref. [15], Copyright 2013 Wiley)

synthetic hydrogels. The hydrogel templates can be facilely fabricated as described below. The monomer, cross-linker, and initiator with proper concentration were dissolved in ion-exchanged water, and the solution was poured into a glass mold ($10 \times 10 \times 2 \text{ mm}^3$). Then the glass mold was irradiated for 12 h under UV light (365 nm) at room temperature to obtain sheet-shaped hydrogel sample. The hydrogel was first immersed into a large amount of ion-exchanged water for 3 days to extract residual chemical agents. To discuss the correlation between the properties of the synthetic hydrogels and the cell behaviors, we should first characterize the properties of hydrogel exactly under the condition that is similar to cell cultivation. Therefore, the prepared hydrogel samples were then immersed into phosphate buffer saline (PBS) for 3 days, to adjust the pH (7.5) and ionic strength (0.15 M) of the solution contained in the hydrogels. The water and PBS used here should be changed every day. After these treatments, a hole punch was used to punch sheet-shaped hydrogel into disk shape (15 mm or 34 mm diameter). These disk-shaped hydrogel samples were sterilized by autoclave (120 °C, 20 min) in PBS and then were transferred into 24-well or 6-well tissue culture polystyrene (TCPS). After equilibrated by DMEM for 24 h, these samples can be used as templates for cell seeding (Scheme 2.1). Unlike other artificial templates, in our approach, the hydrogel templates were not modified by any cell-adhesive proteins or peptides, offering several advantages, such as capability to discuss the correlation between the physicochemical properties

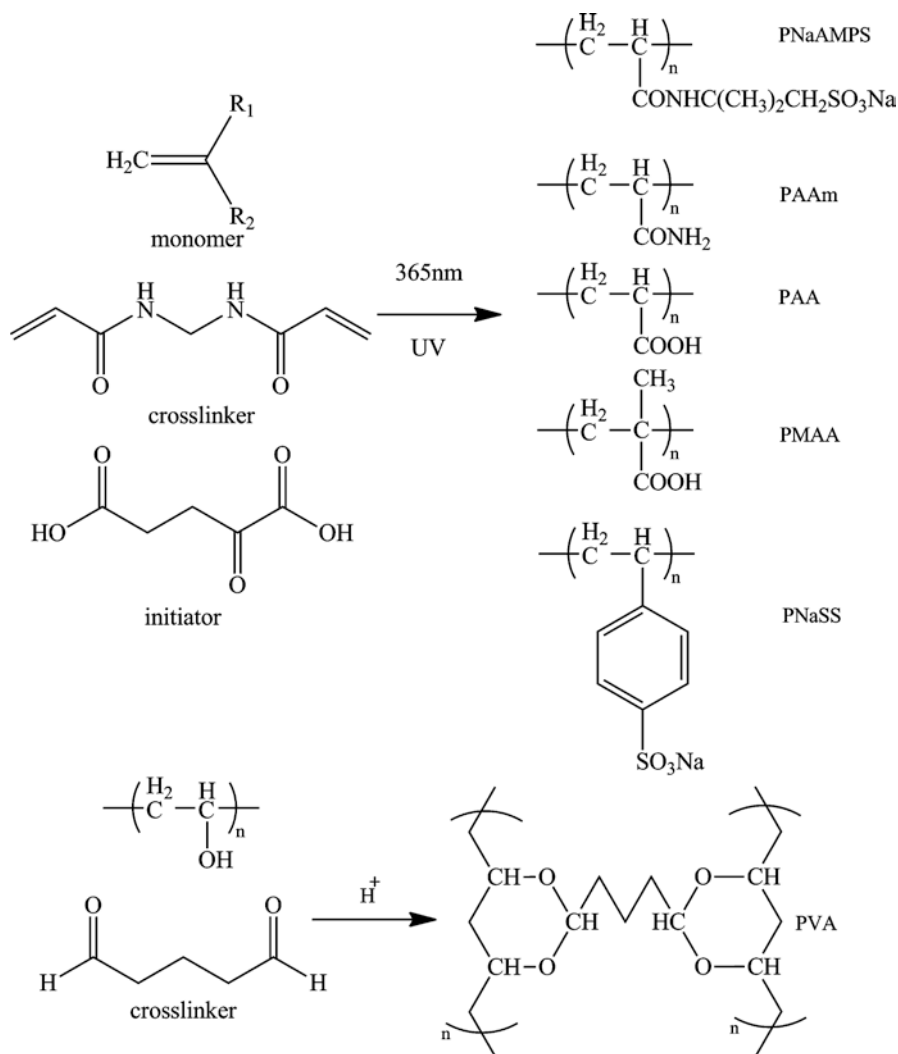
(e.g., chemical structure, Young's modulus, and zeta potential) of synthetic hydrogels and cell behaviors, good reproducibility, free of infection, tolerance for high-temperature sterilization, and relatively low cost.

The cells used in our projects were first subcultured on the TCPS until confluent and then were dissociated from the culture plate using 0.05% trypsin-EDTA to obtain cell suspension. Then the cell suspension with exact density was dropped onto the hydrogel surface homogeneously. The cell-seeded samples were cultured at 37 °C in a humidified atmosphere of 5% CO₂. The culture medium was changed every 48 h gently to avoid the damage of the cells and hydrogels. At the proper culture period (6, 24, 48, 72, 96, and 120 h), the cell-loading samples were monitored by taking photos using a phase-contrast microscope equipped with a digital camera to study the morphology and proliferation of the cells. Dynamic cell motility was analyzed as follows. Cell observations were continued for 6–12 h after seeding the cells on the hydrogels, using a CCD camera, and the images were analyzed using a computer program (MetaMorph). The migration velocity of the cells is defined as the ratio of the distance of cell migration and culture time. Cell area can be measured from images by tracing cell boundaries.

2.3 Effect of Chemical Structure on Cell Behaviors

Many physicochemical properties of templates affect cell adhesion, spreading, and proliferation, such as chemical structures, Young's modulus, charge density, interfacial energy, hydrophobicity/hydrophilicity balance, mobility of polymer chain, and topology [1, 14, 19, 21–24]. In order to understand the effect of chemical structure on the behaviors of endothelial cells, we cultured endothelial cells on the synthetic hydrogels with different chemical structures, for example, neutral hydrogels without ionized group, including poly(vinyl alcohol) (PVA) and poly(acrylamide) (PAAm), weak polyelectrolytes, poly(acrylic acid) (PAA) and poly(methacrylic acid) (PMAA) with pH-dependent dissociated charged groups, carboxylic group, as well as strong polyelectrolytes, poly(sodium *p*-styrene sulfonate) (PNaSS), and poly(2-acrylamido-2-methyl-1-propanesulfonic sodium) (PNaAMPS), which have fully dissociated charged groups, sulfonate groups (Scheme 2.2).

In order to discuss the effect of chemical structure on cell behaviors, we should clear the interference of the two key parameters, i.e., water content (expression in terms of swelling degree, q , which is defined as the weight ratio of the swollen hydrogel to the dried hydrogel [14]) and Young's modulus, E , on cell behaviors, because they are dependent on chemical structure and cross-linking concentration, M (mol% cross-linking agent in relative to the monomer concentration). The samples with same M but various chemical structures exhibit quite different q and E due to different hydrophilicity and reactivity of monomer species, and the samples with same chemical structure but various M , show diverse q and E due to distinct mesh size of polymer networks [15]. Through statistical analysis, we could not find a clear



Scheme 2.2 The chemical structures of synthetic hydrogels, PNaAMPS, PAAm, PAA, PMAA, PNaSS, and PVA

correlation between the expanded cell number and q . Moreover, according to scaling theory, for a non-charged neutral hydrogel with Gaussian distributed partial chains, E and q obey a scaling relationship of $E \sim q^{-3}$. Considering a high ionic strength ($I = 0.15$) in cell culture medium, the negatively charged hydrogels also approximately obey the scaling relationship, because dissociated counterions dangled on the polymer chains of charged hydrogels are screened. In addition, literatures reported that anchorage-dependent cells proliferate well with the increase of Young's modulus from ~ 1 to ~ 10 kPa [16]. Accordingly, for the present hydrogel-based cell

culture system in which Young's modulus is in the range of 50.0–250.0 kPa, we can assume that cell proliferation is also not correlated with Young's modulus of the hydrogels equilibrated in cell culture medium. This is confirmed by our experiments that the behavior of cell proliferation does not obviously change when $E = 10\text{--}200$ kPa. Therefore, in this contribution, we can discuss the effect of chemical structure of hydrogels on cell behaviors without considering the interference of E and q .

2.3.1 Cell Adhesion, Spreading, and Morphology

Before 6 h of cultivation, endothelial cells do not proliferate but adhere or spread onto templates. Cell spreading ratio and adhesive ratio are parameters which describe cell survival state. Here, the spreading ratio is the number percentage of cells with fusiform or polygonal shape having pseudopodia to the seeded cells on hydrogel surface, while the adhesive ratio represents number percentage of the cells more or less tightly stick to hydrogel surface but maintain spherical shape to the seeded cells [14, 21]. In the stage of initial culture (6 h), chemical structures of hydrogels do not have a remarkable influence on cell adhesion. The sum of adhesive ratio and spreading ratio is higher than 50%. On the other hand, cell spreading and morphology are remarkably influenced by the chemical structure and cross-linking concentration (M) [14]. The morphologies of BFAECs cultured on the hydrogels with various cross-linking concentrations, i.e., PAAm ($M = 1, 2, 3, 4, 6$ mol%), PVA ($M = 1, 2, 4, 6, 10$ mol%), PAA ($M = 1, 2, 4, 6$ mol%), PMAA ($M = 1, 2, 3, 4, 6$ mol%), PNaSS ($M = 4, 6, 8, 10$ mol%), and PNaAMPS ($M = 1, 2, 3, 4, 5, 6$ mol%) at 6 h, are shown in Fig. 2.1a. The corresponding typical phase-contrast micrographs of the BFAECs cultured on the hydrogels with various M , i.e., PVA ($M = 6$ mol%), PAA ($M = 2$ mol%), PMAA ($M = 1$ mol%), PNaSS ($M = 10$ mol%), and PNaAMPS ($M = 6$ mol%), are shown in Fig. 2.1b. It is reported that for the neutral PAAm hydrogels, cell activity is reduced due to the weak interaction between proteins and PAAm [25]. Thus, PAAm hydrogel strongly inhibits cell spreading, most cells adhered on the surface of PAAm hydrogel show spherical morphology, and only 18% cells spread on 4 mol% PAAm hydrogel. Cell compatibility of PVA hydrogel is better than that of PAAm, and ~50% of the adhered BFAECs spread with a few irregular protrusions on the high cross-linked hydrogel ($M = 6, 10$ mol%), whereas it decreases to ~15% for low cross-linked hydrogel ($M = 2, 4$ mol%).

For weak negatively charged hydrogels, the behaviors of cell spreading and morphology are obviously dependent on M . In the case of PAA hydrogel, ~60% and 46% of cells with a morphology of fusiform or polygonal shape spread on the surface of loosely cross-linked hydrogel ($M = 1, 2, 4$ mol%); however, spreading ratio decreases to 23% when M increases to 6 mol%. For PMAA hydrogel, ~50% cells spread on the surface of loosely cross-linked hydrogel ($M = 1, 2, 3$ mol%), whereas it should be mentioned that nearly all spreading cells disappear when M is increased to 4 mol%. It is noteworthy that only strong polyelectrolyte hydrogels facilitate cell

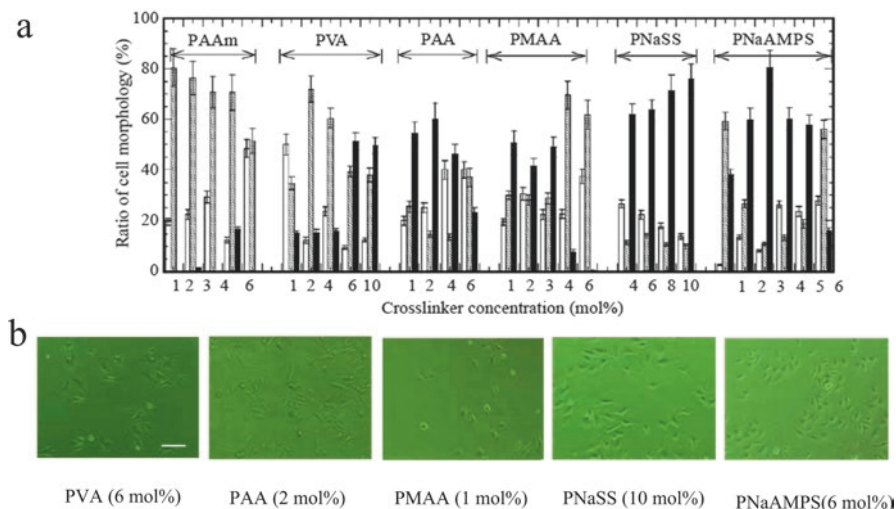


Fig. 2.1 (a) Cell morphologies on PAAm, PVA, PAA, PMAA, PNaSS, and PNaAMPS hydrogels with various cross-linker concentrations at 6 h. (b) Typical phase-contrast micrographs of BFAECs cultured for 6 h on the hydrogels with various cross-linking concentrations, PVA (6 mol%), PAA (2 mol%), PMAA (1 mol%), PNaSS (10 mol%), and PNaAMPS (6 mol%). (Reprinted with permission from ref. [14], Copyright 2005 Elsevier)

activity and the cells with the extension of pseudopodia around their fusiform or polygonal shape spread well on the hydrogels in a wide range of cross-linking concentration ($M = 2-10$ mol%). For PNaAMPS hydrogel, the spreading ratio is higher than 60% when $M = 2, 3, 4, 5$ mol%. While for PNaSS hydrogel, the spreading ratio is 62% for 4 mol% sample, and it increases to 76% for 10 mol% sample.

2.3.2 Cell Proliferation

In the process of prolonged cultivation, cell proliferation strongly depends on the chemical structure and cross-linking concentration of hydrogels. The order of synthetic hydrogels facilitating the proliferation of endothelial cell is as follows: strongly charged hydrogels (PNaAMPS, PNaSS) > weakly charged hydrogels (PAA, PMAA) > neutral hydrogels (PVA, PAAm) [14]. The proliferation (Fig. 2.2a) and cell number (Fig. 2.2c) of BFAECs cultured on the synthetic hydrogels with various chemical structures are shown in Fig. 2.2, in which type I collagen hydrogel is used as positive control. The typical phase-contrast micrographs of BFAECs cultured for 120 h on the hydrogels with diverse M , i.e., PVA ($M = 6$ mol%), PAA ($M = 2$ mol%), PMAA ($M = 1$ mol%), PNaSS ($M = 10$ mol%), and PNaAMPS ($M = 6$ mol%), are shown in Fig. 2.2b. The strong negatively charged hydrogels exhibit the best cell expansion behavior, and the behavior of cell proliferation is similar in a wide range of cross-linking concentration ($M = 2-10$ mol%). For

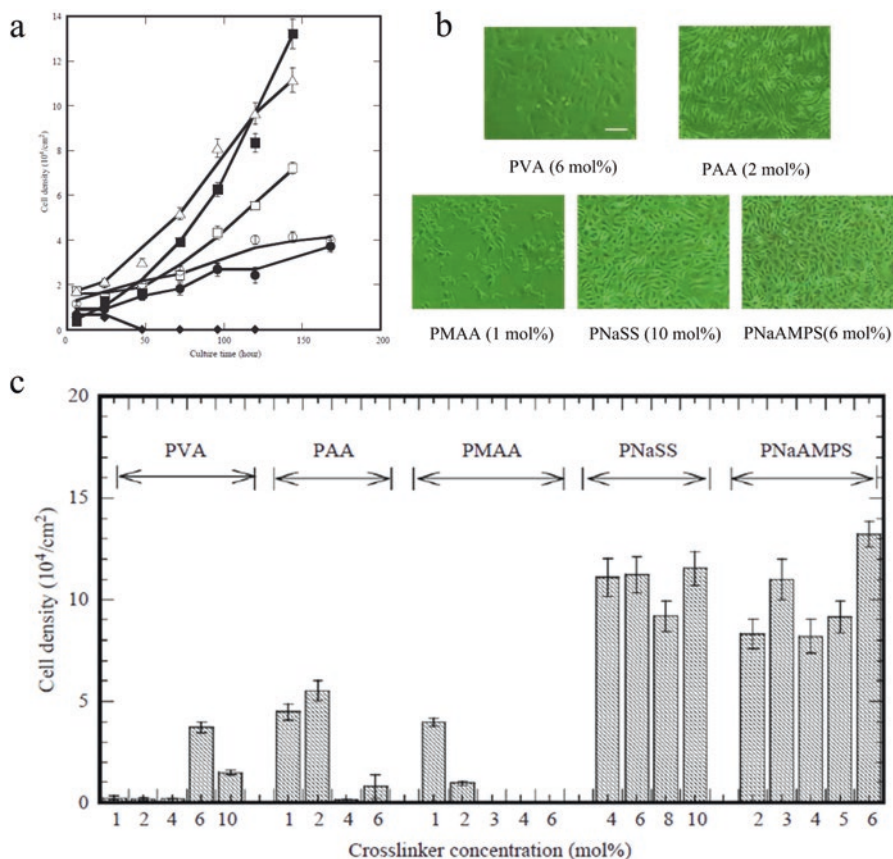


Fig. 2.2 (a) Proliferation of BFAECs on the surface of synthetic hydrogels. (b) Typical phase-contrast micrographs of BFAECs cultured for 120 h on the hydrogels with various cross-linking concentrations, PVA (6 mol%), PAA (2 mol%), PMAA (1 mol%), PNaSS (10 mol%), and PNaAMPS (6 mol%). (c) Density of cells that proliferate to confluent or sub-confluent on various kinds of hydrogels as a function of cross-linking concentration. (Reprinted with permission from Ref. [14], Copyright 2005 Elsevier)

example, cell proliferation on PNaSS hydrogel with $M = 4, 6, 8$ mol% is close to that of 10 mol% PNaSS hydrogel, and cell proliferation on PNaAMPS hydrogel with $M = 2, 3, 4,$ and 5 mol% is similar to that on 6 mol% PNaAMPS hydrogel. After cultivation for 144 h on the surfaces of PNaSS and PNaAMPS hydrogels, the cells proliferate to confluent monolayers with a cell density of $\sim 1.1 \times 10^5$. Cell proliferation and number of expanded cell are close to those on collagen hydrogel. On the other hand, cell proliferation on the weak negatively charged hydrogels is obviously lower than that of strong negatively charged hydrogels, and cell proliferation behavior is clearly dependent on cross-linking concentration. For example, when cross-linking concentration is low ($M = 1, 2$ mol%), cells slowly proliferate with culture time and eventually reach confluence, with a cell density of 6.6×10^4 and

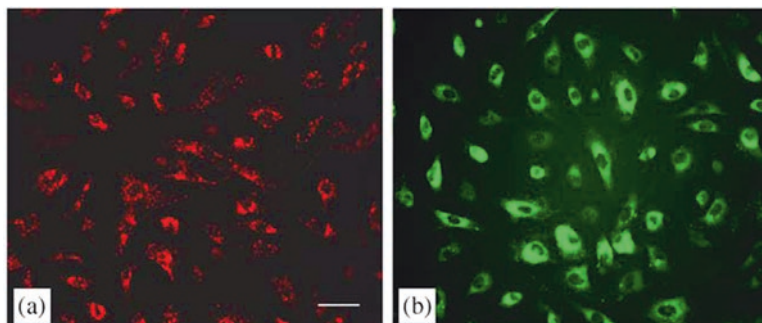


Fig. 2.3 Identification of endothelial cells proliferated on the surface of PAA hydrogels by Dil-Ac-LDL metabolic dye (a) and intracellular vWF (b). Scale bar: 50 μm . (Reprinted with permission from Ref. [14], Copyright 2005 Elsevier)

7.21×10^4 cell/cm² at 144 h, respectively. However, when cross-linking concentration increases to a high value ($M = 4, 6$ mol%), the number of spreading cell gradually decreases with cultivation time, and eventually, nearly no cells proliferate. It has reported that PAA-grafted surface exhibits poor performance of cell adhesion, spreading, and proliferation [26]. Our results demonstrate that PAA hydrogel is able to promote cell expansion when it is cross-linked in a suitable low concentration, because ionization of carboxylic groups dangled on weakly charged polymer chains increases with a decrease of cross-linking concentration and vice versa. The charge density which depends on the cross-linking concentration of PAA hydrogel affects cell behaviors. The details correlated with the zeta potential of hydrogel will be discussed in Sect. 2.4.1. For nonionic hydrogels, cell proliferation is poor, and the behaviors of cell proliferation on nonionic hydrogels obviously depend on chemical structure and cross-linking concentration. When PVA hydrogel is densely cross-linked ($M = 6, 10$ mol%), the cells proliferate with culture time and reach sub-confluence for 168 h, with a low cell density of 3.72×10^4 and 2.67×10^4 cell/cm², respectively, whereas the cells cannot proliferate with culture time when PVA hydrogel is loosely cross-linked ($M = 2$ and 4 mol%). Unfortunately, the cells cannot proliferate on the PAAm hydrogel cross-linked in the range of 1–10 mol%.

The endothelial cell nature of BFAECs can be confirmed by two kinds of standard methods, i.e., the uptake of 1,1'-dioctadecyl-3,3',3'-tetramethylindocarbocyanine perchlorate (Dil-Ac-LDL) and intracellular staining of the von Willebrand factor (vWF). It is confirmed that the cells expanded on PAA hydrogel maintain their endothelial cell nature. When the cells were subjected to uptake of Dil-Ac-LDL metabolic dye (Fig. 2.3a) and stained for the presence of intracellular vWF (Fig. 2.3b), they exhibited staining with both markers.

Same as BFAECs, proliferation behaviors of other type of endothelial cells, HUVECs, also obviously depend on chemical structure of hydrogels. The order of negatively charged hydrogels facilitating HUVEC expansion is PNaAMPS \approx NaSS >PAA [17]. The proliferation (Fig. 2.4a) and cell number (Fig. 2.4c) of HUVECs

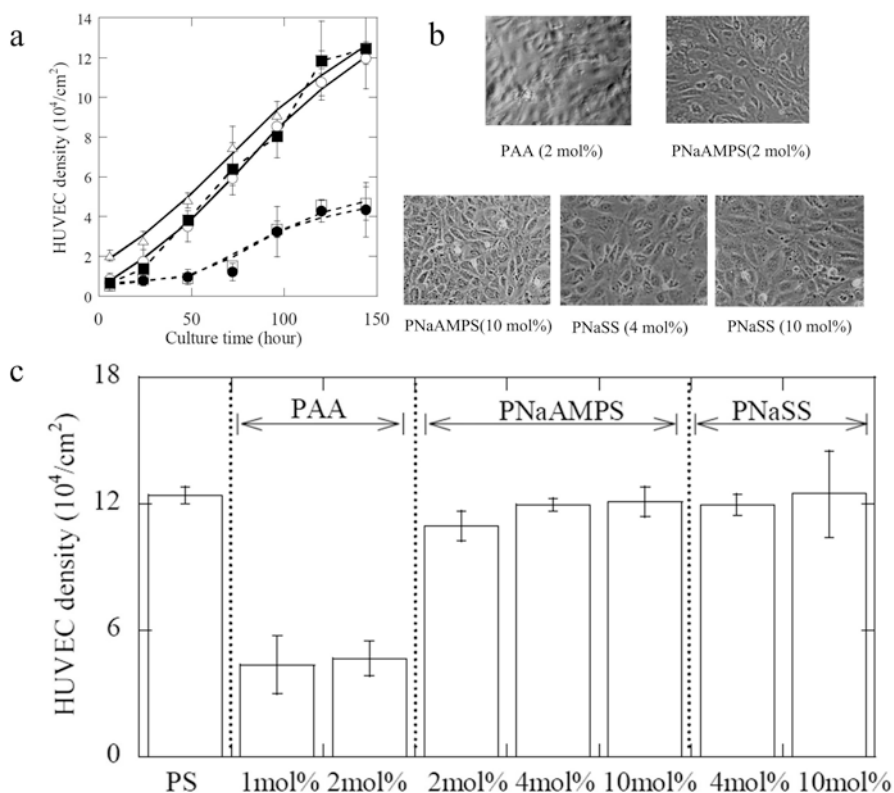


Fig. 2.4 Proliferation (a), typical phase-contrast micrographs (b) and cell density (c) of HUVECs cultured 120 h on the surface of PAA ($M = 1, 2 \text{ mol}\%$), PNaAMPS ($M = 2, 10 \text{ mol}\%$), and PNaSS ($M = 4, 10 \text{ mol}\%$) hydrogels. (Reprinted with permission from Ref. [17], Copyright 2007 Elsevier)

cultured on the synthetic hydrogels with various chemical structures are shown in Fig. 2.4, in which TCPS plate is used as control. The typical phase-contrast micrographs of the HUVECs cultured for 144 h on the hydrogels with diverse chemical structure and cross-linking concentration, i.e., PAA (2 mol%), PNaAMPS (2, 10 mol%), and PNaSS (4, 10 mol%), are shown in Fig. 2.4b. The behaviors of cell proliferation on strong negatively charged hydrogels are similar in a wide range of cross-linking concentration ($M = 2\text{--}10 \text{ mol}\%$). For example, cell proliferation on 4 mol% PNaSS and 10 mol% PNaAMPS hydrogel is close to that of 10 mol% PNaSS and 2, 4 mol% PNaAMPS hydrogels. The fusiform- or polygonal-shaped cells cultured on the PNaAMPS and PNaSS hydrogels proliferate to confluent monolayers with a high cell density of $\sim 1.1 \times 10^5$ for 144 h. Cell proliferation and number of expanded cells are close to those on TCPS plate. However, same as BFAECs, proliferation of HUVEC on the weak negatively charged hydrogels, PAA, is obviously lower than that of strong negatively charged hydrogels. The cells cannot well spread on the PAA hydrogel ($M = 1, 2 \text{ mol}\%$) and slowly proliferate to

sub-confluence for 144 h cultivation, with a cell density of 4.5×10^4 cell/cm². The proteins derived from cell culture medium automatically adhere on the surface of strong negatively charged hydrogels contribute to the behaviors of cell expansion. The details will be discussed in Sect. 2.5.

2.4 Effect of Zeta Potential on Cell Behaviors

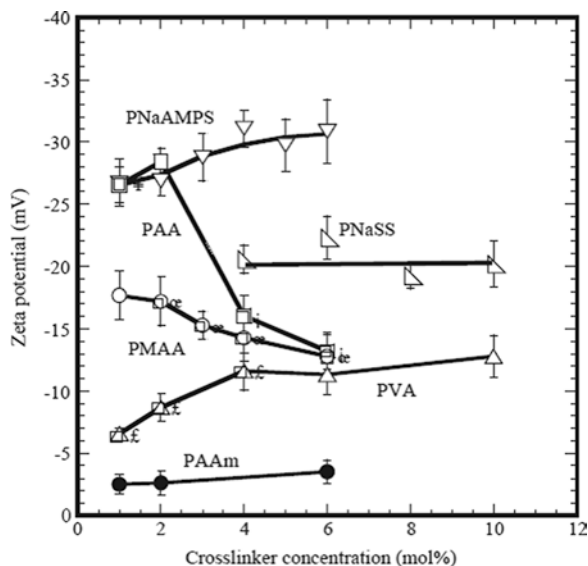
In fact, the interaction between cells and templates is closely related to surface charge of template [27]. Based on the results of the effect of chemical structure and cross-linking concentration on cell behaviors, the behaviors of endothelial cells definitely relate to the surface charge of synthetic hydrogels. That is, zeta potential (ζ) of hydrogel is a vital parameter which affects cell behaviors. Herein, the cell behaviors depending on zeta potential, i.e., static cell behaviors (adhesion, spreading, morphology, proliferation, cytoskeletal structure, and focal adhesion) and dynamic cell behaviors (migration velocity, morphology oscillation), are introduced. Moreover, the relationship between zeta potential and a typical cell-adhesive protein, fibronectin, which is responsible for cell behaviors, is analyzed.

2.4.1 Effect of Zeta Potential on Static Cell Behaviors

2.4.1.1 Effect of Zeta Potential on Cell Morphology and Proliferation

It has been reported that surface charge density affects cell attachment and growth [21, 22]. We discuss the effect of zeta potential of hydrogels with various chemical structures (PVA, PAAm, PAA, PMAA, PNaSS, and PNaAMPS) and cross-linking concentrations, on the behaviors of endothelial cells. The values of zeta potential of negatively charged hydrogels should be negative; thus, a low value represents high charge density and vice versa. The zeta potential of strong negatively charged hydrogels equilibrated in deionized water dramatically decreases with an increase of cross-linking concentration, demonstrating that the charge density of the hydrogels increases with cross-linking concentration. Because water content decreases with an increase of cross-linking concentration, it leads to aggregation of more polymer chains and small mesh size of networks. In fact, in HEPES buffer solution (pH = 7.4) with high ionic strength ($I = 0.15$), the charge of hydrogel is shielded by a large amount of ions. Therefore, the zeta potential of strong polyelectrolyte hydrogels equilibrated in HEPES buffer solution is not obviously dependent on cross-linking concentration. The zeta potential of PNaSS hydrogel shows a value of *c.a.* -20.0 mV which is independent of cross-linking concentration in a large range ($M = 4\text{--}10$ mol%). For another strong polyelectrolyte hydrogel, PNaAMPS, the same phenomena are also observed. The zeta potential of PNaAMPS hydrogel is *c.a.* -30.0 mV when $M = 1\text{--}6$ mol% (Fig. 2.5). The phenomenon is in

Fig. 2.5 Zeta potential of hydrogels as a function of cross-linking concentration in HEPES buffer solution. (Reprinted with permission from Ref. [14], Copyright 2005 Elsevier)

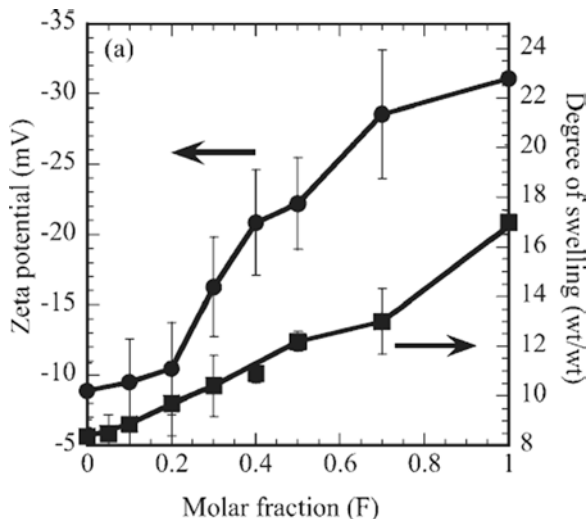


agreement with the results of cell spreading (Fig. 2.1) and proliferation (Fig. 2.2, Fig. 2.4) on PNaSS and PNaMPS hydrogels, which is not sensitive to their cross-linking concentration. The zeta potential of weak negatively charged hydrogels with carboxylic groups, PAA and PMAA, is negative under pH = 7.4, due to the dissociation of carboxylic groups. Their zeta potential is notably dependent on cross-linking concentration, i.e., the zeta potential decreases with a reduction of cross-linking concentration. The mesh size of weak negatively charged hydrogel decreases with an increase of cross-linking concentration, resulting in a decrease in the distance among polymer chains. For maintaining a thermodynamic stability in a small space, the suppression of ionization of carboxylic groups leads to decreased electrostatic repulsion in the hydrogel networks.

The dependence of zeta potential on cross-linking concentration is in agreement with the result of cell proliferation on PAA and PMAA hydrogels, i.e., the cell expansion on PAA and PMAA hydrogels with loosely cross-linked polymer networks is better than that on densely cross-linked polymer networks. For example, 1 and 2 mol% PAA hydrogels with *c.a.* -27.0 mV zeta potential facilitate cell spreading and expansion to sub-confluent. On the other hand, a sharp ascent of zeta potential (*c.a.* -14.0 mV) of 4 and 6 mol% PAA hydrogels cannot support cell expansion. Same as PAA hydrogel, 1 and 2 mol% PMAA hydrogels with *c.a.* -18.0 mV zeta potential support cells extend to sub-confluent, whereas the 4 and 6 mol% PMAA hydrogels with a little high zeta potential (*c.a.* -14.0 mV) cannot support cell extension. In addition, neutral PAAm hydrogel cannot support cell proliferation because it only exhibits a small negative zeta potential due to ionic ion adsorption in the HEPES buffer solution (Fig. 2.5).

Copolymer hydrogels with different charge density, poly(NaAMPS-*co*-DMAAm) and poly(NaSS-*co*-DMAAm), can be used as an ideal model to

Fig. 2.6 The zeta potential and degree of swelling of poly(NaAMPS-*co*-DMAAm) hydrogels as a function of molar fraction F . (Reprinted with permission from Ref. [16], Copyright 2009 Wiley)



systematically analyze the effect of zeta potential on cell behaviors. By adjusting molar fraction, F (the molar ratio of the anionic monomer to total amount of monomers in feed), zeta potential (ζ) of poly(NaAMPS-*co*-DMAAm) and poly(NaSS-*co*-DMAAm) hydrogels can be quantitatively tuned. The charge density of poly(NaAMPS-*co*-DMAAm) hydrogels swollen in HEPES buffer increases with an increase of the amount of negatively charged PNaAMPS, which was confirmed by the increase of absolute value of zeta potential, $|\zeta|$ and q with F (Fig. 2.6) [1]. Here, large $|\zeta|$ denotes more high charge density of the copolymer hydrogels and vice versa.

Then, we analyzed the behaviors of spreading and proliferation of BFAECs and HUVECs cultured on the surface of poly(NaAMPS-*co*-DMAAm) and poly(NaSS-*co*-DMAAm) hydrogels. The spreading ratio of BFAECs at initial culture period (6 h) and cell density at long-term period proliferation (120 h) cultured on poly(NaAMPS-*co*-DMAAm) hydrogels with $F = 0, 0.3, 0.4, 0.5, 0.7, 1.0$ is shown in Fig. 2.7a. The corresponding proliferation kinetics and morphology of the cells are shown in Figs. 2.7b and c (*column I*), respectively. Nearly all BFAECs present spherical morphology when $F = 0$ because of the neutral charged PDMAAm hydrogels. When $F < 0.3$, ~30% BFAECs spread with a few irregular protrusions, but no cell expands with culture time. When $F = 0.3$ – 1.0 , the spreading ratio (40–72%) obviously increases, and the cells present fusiform or polygonal shape with the extension of pseudopodia. The cells further expand with culture time and reach confluent monolayer with cell density of *c.a.* 1.25×10^5 cell/cm² for 120 h. These results indicate that charge density striking affects cell morphology and expansion.

When we plot cell density as a function of the $|\zeta|$ of poly(NaAMPS-*co*-DMAAm) and poly(NaSS-*co*-DMAAm) hydrogels, it shows that there are three stages of cell expansion, i.e., slowly increase stage or nonproliferate stage, rapid expansion stage,

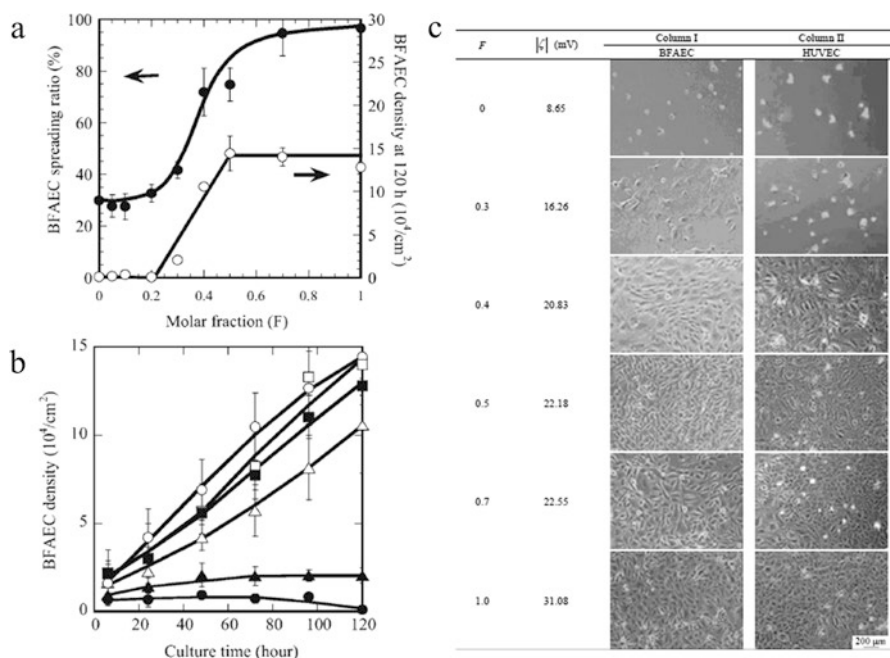


Fig. 2.7 (a) Spreading ratio (6 h) (●) and cell density (120 h) (○) of BFAECs cultured on poly(NaAMPS-co-DMAAm) hydrogels as a function of molar fraction F . (b) Densities of the BFAECs cultured on poly(NaAMPS-co-DMAAm) hydrogels as a function of culture time. (●) $F = 0$, (▲) $F = 0.3$, (△) $F = 0.4$, (○) $F = 0.5$, (□) $F = 0.7$, and (■) $F = 1.0$. (c) Phase-contrast micrographs of BFAECs (column I) and HUVECs (column II) cultured on poly(NaAMPS-co-DMAAm) hydrogels with various molar fraction, F , corresponding to various absolute value of zeta potential, $|\zeta|$. (Reprinted with permission from Ref. [16], Copyright 2009 Wiley)

and stable expansion stage (Fig. 2.8a, b). It is noteworthy that a critical zeta potential, $\zeta_{critical}$, which controls cell expansion, can be clearly revealed (Fig. 2.8c).

When $|\zeta| \leq 16.26$ mV ($F \leq 0.3$), cell expansion is in the stage of slow increase or nonproliferate, most BFAEC and HUVECs exhibit a spherical morphology or slight spreading with a few irregular protrusions, only a few BFAECs expand, and HUVECs are not able to expand on the copolymer hydrogels. When $|\zeta| = 20.83$ mV ($F = 0.4$) – 22.18 mV ($F = 0.5$), cells enter the stage of rapid expansion. All BFAECs and HUVECs spread extensively on the hydrogels, and the cells proliferate to form a confluent monolayer with a cell density of 1.4×10^5 cell/cm² for BFAECs and 1.25×10^5 cell/cm² for HUVECs. Furthermore, when $|\zeta| > 22.18$ mV ($F > 0.5$), all cells expand well, and the cell density maintains the high value which does not obviously change with $|\zeta|$ and saturates to a stable value ($\sim 1.5 \times 10^5$ cell/cm²) (Fig. 2.8a). At this stable expansion stage, both BFAECs and HUVECs expand to form a confluent monolayer with a high cell density. Thus, there is a critical zeta potential, $\zeta_{critical} = -20.83$ mV, controlling cell proliferation on poly(NaAMPS-co-DMAAm),

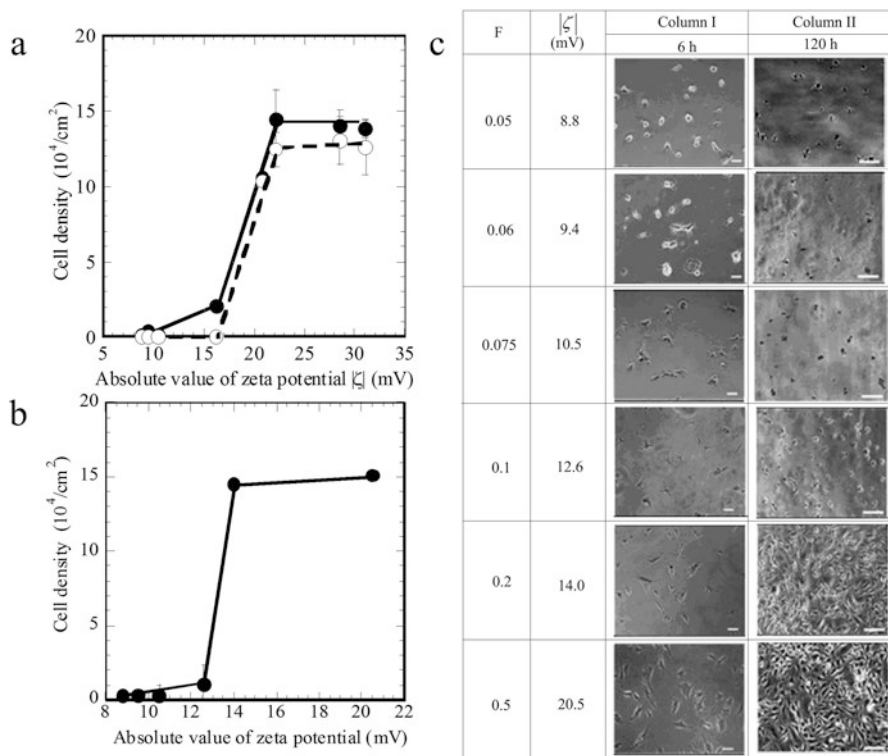


Fig. 2.8 (a) Cell density at 120 h as a function of absolute value of zeta potential, $|\zeta|$, of poly(NaAMPS-co-DMAAm) hydrogels: (●) BFAECs and (○) HUVECs. (b) The BFAEC density on poly(NaSS-co-DMAAm) hydrogel at 96 h as a function of the absolute value of zeta potential, $|\zeta|$. (c) Phase-contrast micrographs of HUVECs cultured on poly(NaSS-co-DMAAm) hydrogels with various zeta potentials at 6 h and 96 h. Scale bar: 100 μm . (Reprinted with permission from Ref. [1, 17], Copyright 2009 Royal Society of Chemistry and 2007 Elsevier)

below which the endothelial cells are able to initially spread and proliferate to form a confluent monolayer over long-term cultivation.

The similar three stages of cell density change and $\zeta_{critical}$ effect also can be observed on the poly(NaSS-co-DMAAm) hydrogels with various F (Fig. 2.8b). At slow increase stage or nonproliferate stage, $|\zeta| \leq 12.6$ mV ($F \leq 0.1$), most BFAECs exhibit a round morphology, and only few cells present slight spreading with a few irregular protrusions at 6 h. However, the cells gradually died with cultivation. At rapid expansion stage, $|\zeta| = 14.0$ mV ($F = 0.2$), most of the cells extensively spread on the copolymer hydrogels, and the cells extend to form a confluent monolayer ($\sim 1.45 \times 10^5$ cell/ cm^2) at 96 h. At stable expansion stage, $|\zeta| \geq 14.0$ mV ($F \geq 0.2$), all cells proliferate to form a confluent monolayer with high cell density of $\sim 1.5 \times 10^5$ cell/ cm^2 . Thus, there is a critical zeta potential, $\zeta_{critical} = -14.0$ mV, controlling BFAEC expansion on poly(NaSS-co-DMAAm) hydrogels. Compared with $\zeta_{critical} (-20.83$ mV) for BFAECs cultured on poly(NaAMPS-co-DMAAm)

hydrogels, the $\zeta_{critical}$ (-14.0 mV) cultured on poly(NaSS-*co*-DMAAm) hydrogels shifts to a higher value. That is, less PNaSS is enough for the expansion of endothelial cells. It is considered that PNaSS with aromatic ring close to the ionizable group facilitates protein adsorption from serum-containing culture medium than that of PNaAMPS [16]. It suggests that both zeta potential and chemical structure affect cell behaviors.

2.4.1.2 Effect of Zeta Potential on Cytoskeleton Structure and Focal Adhesion of Cells

We observed cytoskeleton structure and focal adhesion of BFAECs cultured on the surface of poly(NaSS-*co*-DMAAm) hydrogels. Stress fibers and vinculin are the features of normal strongly adherent cells that are stationary on substrates [28]. Stress fibers organized by microfilaments (F-actin) and non-muscle myosin II play a number of functions including cell adhesion, migration, and morphogenesis. Vinculin is a membrane-cytoskeletal protein constitutes of focal adhesion plaques, which associates with cell-cell and cell-matrix junctions and involves in anchoring F-actin to the membrane. The effect of zeta potential on cell morphology is clearly revealed by the structures of actin fibers and focal adhesion of the BFAECs cultured on poly(NaSS-*co*-DMAAm) hydrogels. The cells are well immobilized on the surfaces of poly(NaSS-*co*-DMAAm) hydrogels with low zeta potential, but not on hydrogels with high zeta potential. The BFAECs are able to form stable focal adhesions on the hydrogel with high $|\zeta|$ value ($|\zeta| = 20.5$ mV). The well-developed actin stress fibers distributed around an individual cell and a complex networks formed by F-actin can be revealed by rhodamine-phalloidin staining. In addition, a large vinculin-containing focal adhesion complexes homogeneously distributed in the cells can be revealed by FITC-conjugated secondary antibody. The cells perform weak adhesion on the hydrogels with low $|\zeta|$ value. When $|\zeta| = 9.4$ mV, cells are deficient in actin stress fibers, and vinculin-containing focal adhesion complexes distribute only around cell edge (Fig. 2.9) [1].

2.4.2 Effect of Zeta Potential on Dynamic Cell Behaviors

Dynamic behaviors of cells play a diversity of roles in a wide variety of biological processes. Cell motility is important in embryogenesis, inflammatory response, wound healing, and the metastasis of tumor cells [29–33]. Investigating the motility of endothelial cells can reveal information on angiogenesis. For example, in order to form capillary sprouts, the activated endothelial cells degrade the underlying basement membrane and migrate and proliferate in the perivascular stroma. In the multistep processes of the formation of new blood vessels, the activated endothelial cells cease proliferation and finally yield new operational blood vessels after the

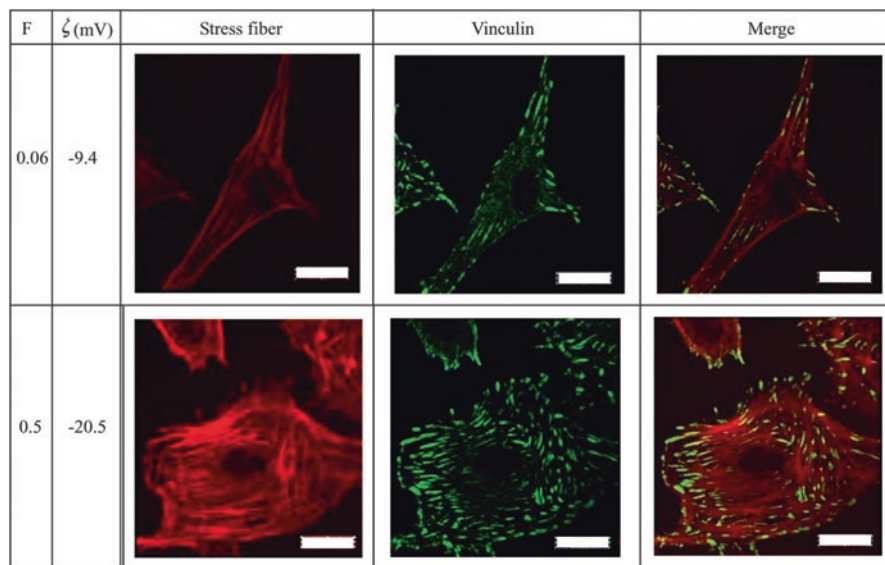


Fig. 2.9 The actin stress fibers and focal adhesions, vinculin, of the BFAECs cultured on poly(NaSS-*co*-DMAAm) hydrogels with $\zeta = 9.4$ mV ($F = 0.06$) and $\zeta = 20.5$ mV ($F = 0.5$). Scale bar: 20 μm . (Reprinted with permission from Ref. [1], Copyright 2009 Royal Society of Chemistry)

processes of sprouting endothelial cells align, form tubes with a patent lumen, and deposit a basement membrane [34, 35]. Herein, the effect of zeta potential on dynamic behavior of endothelial cells including migration velocity, migration distance, and morphology oscillation is discussed.

For understanding the effect of zeta potential of hydrogel on cell dynamic behaviors, Young's modulus (E) of hydrogel which affects cell behaviors should be avoided. For instance, collagen-modified PAAm hydrogel is ordinarily used for studying the effect of Young's modulus on cell motility. However, the effect of zeta potential of hydrogel on cell motility is rarely studied. In order to explore this, we designed the hydrogels with a large range of zeta potential, at the same time, maintaining an identical Young's modulus, through adjusting the content of PNaSS in poly(NaSS-*co*-DMAAm) copolymer hydrogel. We obtain a series of poly(NaSS-*co*-DMAAm) copolymer hydrogels, which $|\zeta|$ is in the large range of 8.8–20.5 mV, and E maintains in 160–198 kPa, by keeping the total monomer concentration at 1 M and cross-linker (MBAA) concentration at 4 mol% while varying the molar fraction (F) of NaSS in a range of 0.05–0.5 (Fig. 2.10a). We found that the charge density of hydrogel remarkably affects migration velocity of endothelial cells. The average migration velocity of BFAECs cultured on poly(NaSS-*co*-DMAAm) hydrogels from 6 to 12 h as a function of zeta potential is shown in Fig. 2.10b. The spreading area of cells corresponding with migration velocity is also clearly demonstrated. According to the relationship between migration velocity and cell area, we can find

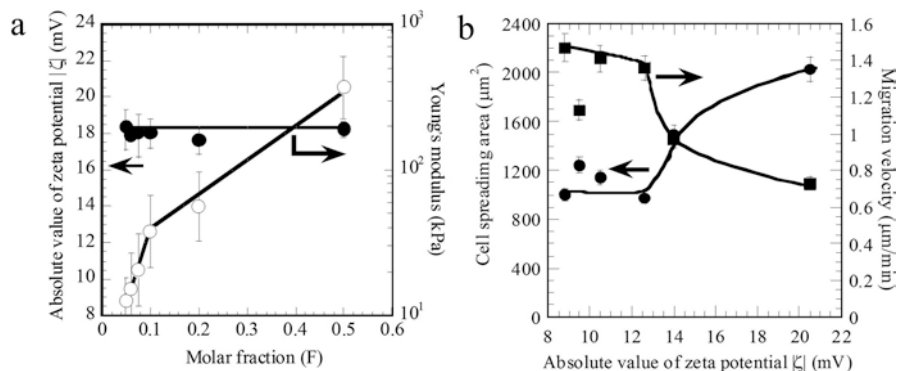


Fig. 2.10 (a) The absolute value of zeta potential ($|\zeta|$) (○) and Young's modulus (E) (●) of poly(NaSS-co-DMAAm) hydrogels as a function of molar ratio ($F = 0.05$ – 0.5). (b) The spreading area and the average migration velocity of the BFAECs cultured for 6–12 h as a function of the poly(NaSS-co-DMAAm) copolymer hydrogels. (Reprinted with permission from Ref. [1], Copyright 2009 Royal Society of Chemistry)

that the migration velocity of the cells is closely related to their shape; extensively spreading cells migrate slowly and vice versa. The detailed information is described as follows. The migration velocity of BFAECs decreases with $|\zeta|$, and the cells exhibit an abrupt decrease in migration velocity at $\zeta_{critical} = -14.0$ mV. When 8.8 mV $< |\zeta| < 12.6$ mV ($F = 0.05$ – 0.1), average migration velocity is the fastest (~ 1.5 $\mu\text{m}/\text{min}$), whereas the corresponding spreading area is the minimum (~ 1000 μm^2). When $|\zeta| = 14.0$ mV ($F = 0.2$), migration velocity dramatically drops to 0.97 $\mu\text{m}/\text{min}$, while spreading area increases to 1496 μm^2 . With further increase $|\zeta|$ to 20.5 mV ($F = 0.5$), migration velocity decreases to the minimum (0.73 $\mu\text{m}/\text{min}$), and spreading area increases to maximum (2028 μm^2).

We further analyze the motility of a single cell cultured on the hydrogel. It is noteworthy that when 8.8 mV $< |\zeta| < 12.6$ mV ($F = 0.05$ – 0.1), the BFAECs perform the maximum migration velocity on the poly(NaSS-co-DMAAm) hydrogel but do not proliferate. The single cell repeatedly changes its morphology and demonstrates periodic morphology oscillation in a stick-slip mode. Cell shape factor (S) which is defined as $S = 4\pi A/P^2$ is used to evaluate the change of cell morphology, where A is the area occupied by the cell and P is the perimeter of the cell. The cells exhibit a spherical shape when $1-S$ is close to 0, whereas the cells exhibit a spreading shape when $1-S$ is close to 1. The value of $1-S$ dramatically oscillates over a wide range (0 – 1) with culture time (6–12 h). The morphology of the cells repeatedly changes from a spherical shape within 1 min to a spreading shape within ~ 20 min. The longtime difference between cell spreading and shrinkage implies that the polymerization of actin fibers of stress fiber takes a longer time than depolymerization. The average period of cell shape oscillation is 36 min (Fig. 2.11), which is shorter than that of the cells cultured on a substrate-coated low concentration of RGD-containing nanopptide [36]. It is speculated that the following two reasons are related to the phenomenon: (1) the difference of time period of polymerization and collapse of

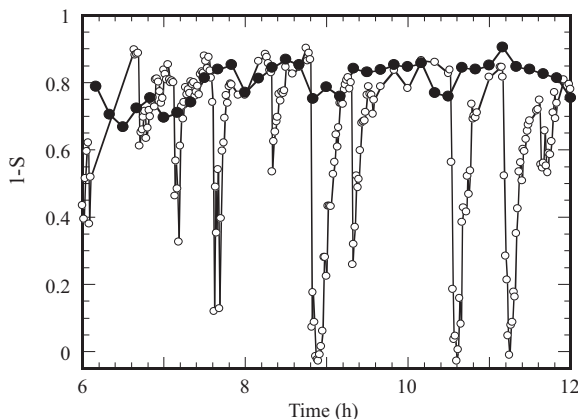


Fig. 2.11 The morphological parameter ($1-S$) of the BFAECs cultured on poly(NaSS-co-DMAAm) hydrogels as a function of culture time. A round shape corresponds to $1-S \rightarrow 0$, and a spreading shape corresponds to $1-S \rightarrow 1$. (○) $|\zeta|=9.4$ mV ($F = 0.06$) and (●) $|\zeta|=20.5$ mV ($F = 0.5$). (Reprinted with permission from Ref. [1], Copyright 2009 Royal Society of Chemistry)

actin fibers and (2) the distinction of cell adhesive force at the sites of focal adhesion on hydrogel in the period of cell spreading and shrinkage.

When $|\zeta| = 9.4$ mV ($F = 0.06$), the shape oscillation of a typical BFAEC cultured on the poly(NaSS-co-DMAAm) hydrogel is monitored by time-lapse video microscopy (Fig. 2.12). A cell rapidly changes from an extensively spreading morphology to a round shape, along with fast shrinkage of filopodia within 1 min (Fig. 2.12–2), and then migrates to another location (Fig. 2.12–3). The migration distance is ~ 700 μm , which is obviously longer than that on the hydrogel with low zeta potential ($|\zeta|=20.5$ mV, $F = 0.5$). Because the cells cultured on the hydrogel with high zeta potential demonstrate poorly developed actin fibers and unstable focal adhesions, the cell fast releases from the pre-existing adhered site when cultured on the hydrogel with high zeta potential. On the other hand, the cells cultured on hydrogel with low zeta potential exhibit well-developed actin fibers and large focal adhesions. After location transformation, the cell develops lamellipodia in the new location for ~ 10 min (Fig. 2.12–11), along with gradual growth of filopodia after pseudopodia formation at 15 min (Fig. 2.12–16). The lamellipodia and filopodia continue to grow until the cell recovers its morphology of extensive spreading (Fig. 2.12–32) [1]. The oscillatory behavior from spherical to spreading shape can persist for many hours at a nearly constant frequency. It is noteworthy that the cell is not able to divide during the process of morphological change, indicating that the change in cell morphology is not associated with mitosis. The know-how of tuning cell behaviors by controlling charge density of hydrogels potentially can be broadly applied to design polymer materials with desired functions in biomedical field.

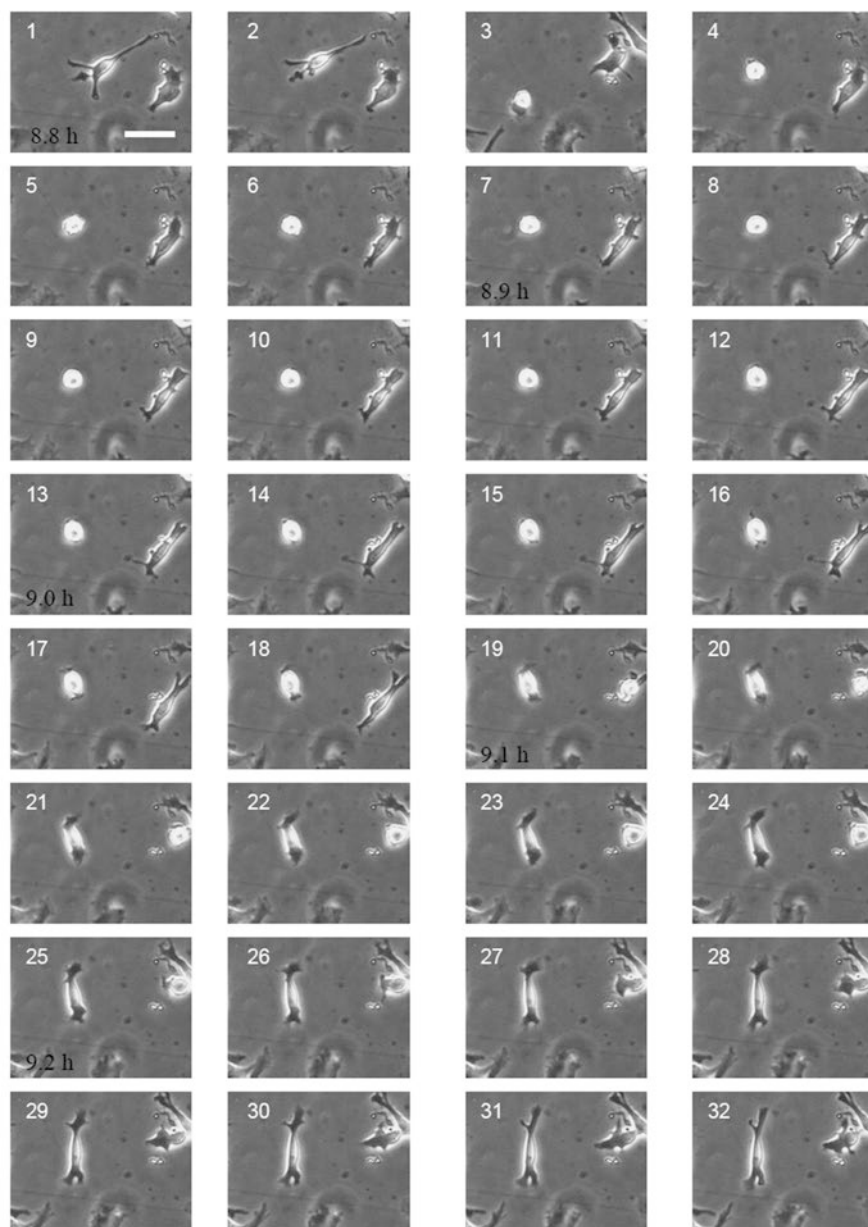


Fig. 2.12 A typical example of morphology change of a single BFAECs cultured on the poly(NaSS-co-DMAAm) hydrogel with $|\zeta|=9.4$ mV at 8.8–9.3 h recorded by CCD camera. The arrows show a single cell repeatedly changing from a spreading morphology to a round shape and then changing back to spreading morphology with time. Time interval between successive images: 1 min. (Reprinted with permission from Ref. [1], Copyright 2009 Royal Society of Chemistry)

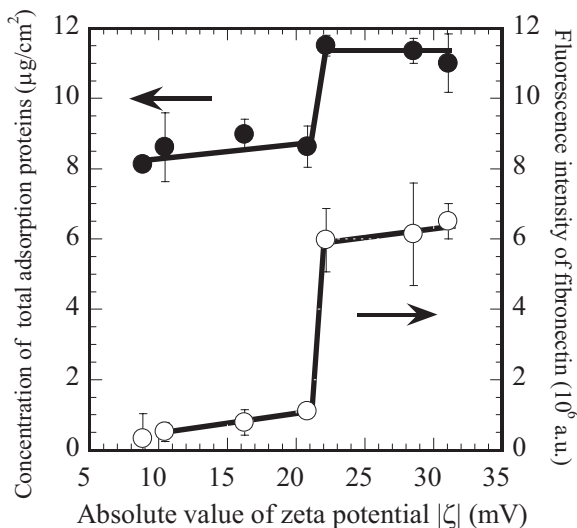
2.5 Relationship of Cell Behaviors and Protein Adsorption

The investigation results of the effect of chemical structure and zeta potential on static cell behaviors (cell proliferation, morphology, cytoskeleton structure, focal adhesion) and dynamic behaviors (migration velocity, migration distance, and morphology oscillation) demonstrate that zeta potential of hydrogels has a profound effect on the behaviors of endothelial cells. Moreover, the endothelial cells prefer to proliferate onto the hydrogels with more negative charges (i.e., zeta potential lower than $\zeta_{critical}$). It is noteworthy that the surface of endothelial cells is also negatively charged, because they are decorated with a high density of polyanionic macromolecules. The endothelial cells are covered by a layer of glycocalyx consisting of proteoglycans and acid glycoproteins dangling of sulfated, carboxylated, or sialic containing residues [37]. It is reasonable to consider that there is no direct electrostatic interaction between endothelial cells and hydrogels which both have negative charges. Thus, we should answer a question, that is, why endothelial cells can spread and proliferate onto the negatively charged hydrogels. It is well known that the adhesive proteins contained in fetal bovine serum (FBS) play an important role in tuning the behaviors of anchorage-dependent cells [15, 38]. We hypothesized that the adhesive proteins contained in cell culture medium may easily adhere onto the surface of negatively charged hydrogels and further influence cell behaviors, because they are amphoteric polyelectrolytes with both acidic and basic peptides. In order to verify this hypothesis, we further analyzed the correlation between the adsorption of a typical cell-adhesive protein contained in FBS, fibronectin, and charge density, using the poly(NaSS-*co*-DMAAm) hydrogels with various charge densities as a model. Fibronectin is a major cell surface receptor anchored onto the interface of template-cell gaps. Cell behaviors will be affected when the transmembrane integrin receptors of a cell are recognized by fibronectin proteins and further activate a cascade of intracellular signaling pathways [38]. Fibronectin plays a critical role in control cell behaviors, for instance, affecting the rate and anisotropism of cell spread, cell-template adhesive force, and migration velocity, as well as stimulating tubular morphogenesis [35, 39].

We found that the charge density of hydrogels adjusts protein adsorption, which further affects cell behaviors. That is, more proteins adsorb onto the hydrogels with high negative charge, favoring cell spreading and proliferation, leading to low migration velocity. On the other hand, only a small amount of proteins adsorb onto the hydrogels with high negative charges, which is poor for cell spreading and proliferation, and the spread cells exhibit high migration velocity. The reasonable answer is as follows. The serum proteins contained in the culture medium can adsorb onto the surface of hydrogels with negative charge by electrostatic interactions. Thus, the adsorbed serum proteins, such as fibronectin, can serve as a “bridge” to induce cell adhesion, spreading, and proliferation onto the negatively charged hydrogels.

Similar to the relationship between cell density and $|\zeta|$, three-stage phenomenon is also observed when we plot the concentration of total adsorbed proteins (C_p) and fluorescence intensity of fibronectin (F_f) as a function of $|\zeta|$ of the poly(NaAMPS-*co*-DMAAm) copolymer hydrogels. In detail, in the stage of slowly adsorption, $|\zeta| \leq 16.26$ mV ($F \leq 0.3$), both C_p and F_f sustain low values and slowly increase with $|\zeta|$.

Fig. 2.13 The concentration of total adsorbed proteins (●) and fluorescence intensity of adsorbed fibronectin (■) on poly(NaAMPS-co-DMAAm) copolymer hydrogels as a function of absolute value of zeta potential $|\zeta|$. (Reprinted with permission from Ref. [1], Copyright 2009 Royal Society of Chemistry)



In the stage of rapid adsorption, $|\zeta| = 20.83$ mV ($F = 0.4$), the values of C_p and F_f dramatically increase to the maximum values. In the stage of stable adsorption, $|\zeta| > 20.83$ mV ($F > 0.4$), the values of C_p and F_f maintain at a stable high values, which are nearly not affected by $|\zeta|$ (Fig. 2.13). The behaviors of actin stress fibers and focal adhesions of endothelial cells clearly reflect the fibronectin adsorption (Fig. 2.9). When being cultured on the surface of hydrogel with high protein adsorption ($|\zeta| = 20.5$ mV), the cells tightly and stably adhere onto the hydrogels with rich fibronectin adsorption. The phenomenon is confirmed by cell behaviors, for example, the cells proliferate with well-developed actin fibers and large focal adhesions, maintaining a stable spreading shape factor. Whereas when cultured on the surface of hydrogel with low protein adsorption ($|\zeta| = 9.4$ mV), the cells are unable to form stable focal adhesions on the hydrogels with poor fibronectin adsorption. For instance, the cells deficient in actin stress fibers and focal adhesions undergo a dramatic oscillation in a stick-slip mode.

2.6 Application of Protein-Free Hydrogels in Biomedical Field

2.6.1 Platelet Compatibility of the Cell Monolayers Cultured on Hydrogel Templates

In vivo, multicellular organisms composed of many kinds of functional cells are supported by other type of cells or ECM [40]. For example, endothelial cells, in charge of procoagulant activity, are living on the ECM composed of vascular smooth muscle cells and type I collagen [41]. It is important to design and fabricate artificial

tissues having the structures similar to in vivo tissues and take full advantages of cell functions. Blood compatibility is one of the basic required parameters of artificial blood vessel, especially for those with small diameters (< 5 mm). In the in vivo vascular systems, endothelial cells inhibit thrombosis by preventing the adhesion of platelets and blood cells onto the wall of vessels. The anticoagulant activity of endothelial cells is dominated by a layer of glycocalyx (0.5–3 mm thickness) which consists of proteoglycans, glycosaminoglycans, and glycoproteins [17, 42, 43]. It is reasonable to consider that artificial blood vessels fabricated with inner endothelial cell monolayer are expected to inhibit thrombosis. However, the blood compatibility of in vitro cultured endothelial cells is poorly investigated [44]. It is a question; do the in vitro cultured endothelial cells have the same antithrombogenic function as that of in vivo living cells? As revealed by the adhesion test of human platelet in static conditions, our works found that the monolayers of HUVECs and HCAECs cultured on synthetic hydrogels exhibit excellent antiplatelet behaviors, compared with the cell monolayer cultured on TCPS. The HUVECs or HCAECs cultured on the surface of hydrogels are denoted as HUVEC/HCAEC-hydrogel (PNaSS, PNaAMPS, PAA) [17]. The platelet adhesion strongly depends on the chemical structure and Young's modulus (E) of synthetic hydrogels, the templates for HUVECs and HCAECs cultivation, controlling the secretion of glycocalyx by the cultured endothelial cells.

In the case of HUVECs cultivated for 144 h, the cells can proliferate and form a monolayer on the strong negatively charged hydrogel, PNaSS ($M = 4, 10$ mol%) and PNaAMPS ($M = 2, 10$ mol%), with a cell density of $\sim 1.2 \times 10^5$ cell/cm², which is close to that cultured on the TCPS plate. The cells cultured on diverse hydrogels exhibit different behaviors of platelet adhesion. The antiplatelet adhesion of the HUVECs cultured on the hydrogel templates increases in the order of HUVEC-PNaSS > HUVEC-PNaAMPS > HUVEC-PAA.

It is noteworthy that HUVEC-PNaSS exhibits the best behavior of antiplatelet. Nearly no platelet adheres on the HUVEC-PNaSS, regardless of the M of the hydrogels [17]. The density of adhered platelets (D_p) on the HUVEC-PNaAMPS dramatically decreases with an increase of the M . D_p is 183×10^4 and 6×10^4 platelet/cm², for $M = 2$ and 10 mol% samples, respectively. While a large amount of platelets (115×10^4 platelet/cm²) adhere onto the HUVECs proliferated to sub-confluent on weak negatively charged PAA hydrogels ($M = 1, 2$ mol%) (Fig. 2.14), on the contrary, a large amount of platelets adhere onto the HUVECs cultured on TCPS.

Same as HUVECs, HCAECs also can proliferate to confluence on the PNaSS hydrogels ($M = 4, 6, 8, 10, 13, 15$ mol%, $E = 3.0, 17.0, 40.0, 60.0, 100.0, 263.0$ kPa,) when cultured for 120 h. The cell density of HCAEC-PNaSS is $\sim 1.25 \times 10^5$ cell/cm², and the proliferation behavior does not depend on E (Fig. 2.15). While the elasticity of PNaSS has a remarkable influence on the morphology of HCAECs, the HCAEC-PNaSS shows round morphology when the cells are cultured on very soft ($E < 40.0$ kPa) or very hard (3 GPa) templates but exhibits elliptic shape on the hydrogels with intermediate elasticity (40.0 kPa $< E < 263.0$ kPa). In detail, the HCAECs perform round or polygonal shape when $E = 3, 17, 40$ kPa, $\sim 40\%$ cells perform fusiform or spindle when $E = 60.0$ kPa, and the number percentage of

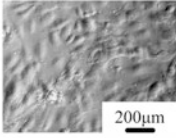
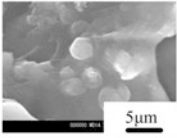
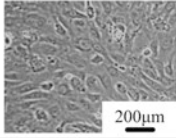
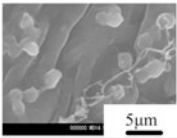
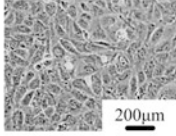
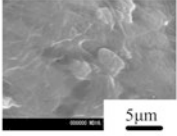
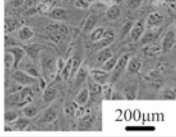
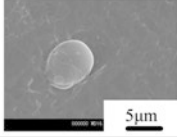
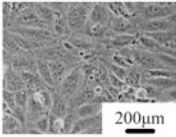
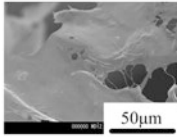
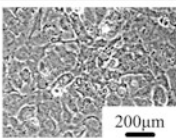
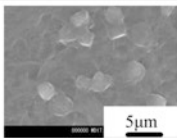
Hydrogels Scaffolds	M (mol%)	Column I	Column II	D_p (10^4 platelet/ m^2)
		HUVEC	Adhered platelet on HUVECs	
PAA	2			115
PNaAMPS	2			183
	10			6
PNaSS	4			0
	10			0
TCPS (Control)	/			185

Fig. 2.14 The typical phase-contrast micrographs of the HUVECs cultured on the various kinds of hydrogels at 144 h (column I), as well as the SEM images (column II) and the density of adhered platelets (D_p) on the corresponding HUVECs. (Reprinted with permission from Ref. [17], Copyright 2007 Elsevier)

fusiform or spindle cells increases when $E = 100.0$ kPa. All cells show spindled morphology when $E = 263.0$ kPa. Platelet adhesion on the HCAEC-PNaSS is obviously dependent on the E and cell morphology. D_p decreases with an increase of E , $D_p = 9.6 \times 10^5$ platelet/ cm^2 for $E = 3.0$ kPa sample, and D_p declines to 1.2×10^5 and 3.0×10^4 platelet/ cm^2 for $E = 60.0, 100.0$ kPa sample, respectively, which is ~ 8 and ~ 30 times lower than that on $E = 3.0$ kPa sample (Fig. 2.15).

The amount of glycocalyx secreted by the HCAECs cultured on the PNaSS hydrogels make us understand the mechanism of the effect of Young's modulus on

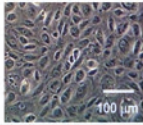
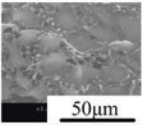
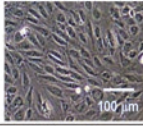
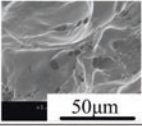
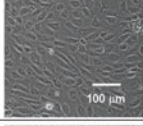
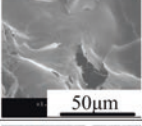
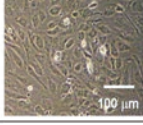
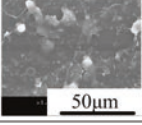
M (mol%)	E (kPa)	HCAEC monolayer	Adhered platelet on HCAECs	Relative RNA of core proteins in GAG			Relative amount of GAG	D_p (10^4 platelet / μm^2)
				glypican	syndecan-4	perlecan		
4	3			2.3	1.7	2.0	0.5	96
10	60			3.2	2.3	2.6	2.1	12
13	100			3.8	2.4	3.1	2.1	3
TCPS (Control)	3×10^6			1	1	1	1	101

Fig. 2.15 The typical phase-contrast micrographs of HCAECs cultured for 120 h on PNaSS hydrogels with $E = 3.0, 60.0,$ and 100.0 kPa, corresponding $M = 4$ mol%, 10 mol%, and 13 mol%, as well as the relative RNA expressions of the specific core proteins of cultured cells in glyocalyx: glypican, syndecan-4, and perlecan, the relative amount of total GAG and D_p on the corresponding cells. (Reprinted with permission from Ref. [19], Copyright 2010 Mary Ann Liebert)

platelet adhesion. The glyocalyx constitutes a large amount of proteoglycans. Heparan sulfate proteoglycans (HSPGs) are the main component of proteoglycans (50–90%), consisting of core protein and heparan sulfate-type glycosaminoglycan [42, 43]. There are five distinct HSPG core proteins in endothelial cells, i.e., perlecan, syndecan-1, syndecan-2, syndecan-4, and glypican [45]. Perlecan exhibits antithrombin activity by activating antithrombin III via heparin-like sequences in the heparan sulfate chains. Arterial segments with perlecan-expressing endothelial cells completely prevent thrombosis occlusion, while injured arterial segments containing perlecan-deficient cells increase the rate of thrombosis occlusion [46, 47].

To investigate the effect of Young's modulus on glyocalyx secretion, we determined the relative RNA levels of core proteins in HSPGs. Real-time polymerase chain reaction (PCR) showed that perlecan, syndecan-1, syndecan-2, syndecan-4, and glypican were found in the cultured HCAECs. Especially, the amount of perlecan, syndecan-4, and glypican is larger compared with that of syndecan-1 and syndecan-2. Moreover, the amount of specific glyocalyx, glypican, syndecan-4, and perlecan, secreted by the cultured HCAECs, goes up with an increase of the E of the PNaSS hydrogels, which is obviously higher than that of the cells cultured on TCPS.

Accordingly, the mechanism of the effect of Young's modulus on platelet adhesion can be understood as follows. The amount of glycocalyx secreted by the cultured HUVECs and HCAECs is modulated by charge density and Young's modulus of the hydrogels, i.e., suitable negative charge and proper stiffness of hydrogels facilitate the secretion of more glycocalyx by endothelial cells, leading to better antiplatelet. The mechanism is further confirmed by exploring the behavior of platelet compatibility via tuning the amount of glycocalyx on the cultured endothelial cells. The amount of glycocalyx endothelial cells can be enhanced by a cytokine, transforming growth factor β_1 (TGF- β_1), which stimulates the secretion of more HSPGs [48, 49]. TGF- β_1 treatment is able to increase more than 50% of HSPGs on the surface of endothelial cells. For promoting glycocalyx synthesis, HUVECs were incubated in the serum-containing medium with 20 ng/ml TGF- β_1 for 48 h under 37 °C in a humidified atmosphere of 5% CO₂. On the other hand, the amount of glycocalyx can be reduced by a kind of enzyme, heparinase I, via cleaving glycosaminoglycan side chains from HSPGs [50–52]. Heparinase treatments can reduce 45.9% fluorescence intensity associated with heparin sulfate antibody [51]. For reducing glycocalyx, HUVECs were incubated in serum-free medium containing 1.45 U/ml heparinase I for 4 h at 37 °C in a humidified atmosphere of 5% CO₂. The behaviors of platelet adhesion on the TGF- β_1 and heparinase I-treated HUVECs clearly verified that glycocalyx modulation influences the platelet compatibility. On the other hand, after promoting the amount of HSPGs on TGF- β_1 -treated HUVECs, the D_p of HUVEC-PAA sharply declined from 115 to 10 cells/10⁴ mm². In the case of HUVEC-PNaAMPS, the D_p dramatically decreased from 183, 34 cells/10⁴ mm² to 15, 17 cells/10⁴ mm², for $M = 2, 4$ mol% sample, respectively. Although the D_p is only 6 cells/10⁴ mm² for $M = 10$ mol% PNaSS hydrogel, after declining the amount of HSPGs on heparinase I-treated HUVECs, the D_p of HUVEC-PNaSS obviously increased from 0 to 87 and 32 cells/10⁴ mm², for $M = 4, 10$ mol% sample, respectively. Moreover, about 50% of platelets aggregated onto the heparinase I-treated HUVEC-PNaSS, while the platelets randomly distributed on the as-prepared and TGF- β_1 -treated cell monolayers (Fig. 2.16). Therefore, for the as-cultured HUVECs easily inducing platelet adhesion, platelet compatibility can be obviously improved through increasing the amount of glycocalyx. On the other hand, for the cultured HUVECs rejecting platelet adhesion, platelet compatibility can be seriously induced via decreasing the amount of glycocalyx. It can be inferred that the HUVEC monolayers cultured on the PNaSS ($M = 4, 10$ mol%) hydrogel, which do not induce platelet adhesion, secreting rich HSPGs, yet the HUVECs cultured on the PAA ($M = 1, 2$ mol%) and PNaAMPS ($M = 2$ mol%) hydrogels, which induce the adhesion of a large amount of platelets, have poor HSPGs. The results demonstrate that it is possible to fabricate hybrid artificial blood vessel with high blood compatibility, by using PNaSS hydrogel with platelet compatible endothelial cell monolayer as its inner surface.

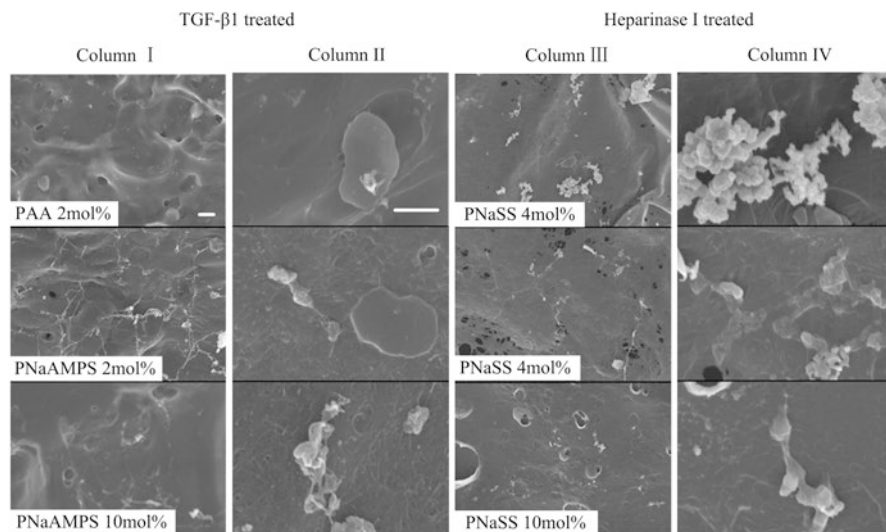


Fig. 2.16 The SEM images of the adhered platelets on the HUVECs cultured on various kinds of gels treated by TGF- β 1 or heparinase I. Columns II and IV are the magnified images of columns I and III, respectively. Scale bar: 5 μ m. (Reprinted with permission from Ref. [17], Copyright 2007 Elsevier)

2.6.2 Surface Friction of EC Monolayers Cultured on Hydrogel Templates

It is well known, besides inhibition of platelet adhesion, the glycocalyx decorated on the surface of endothelial cells performs vital functions in blood fluid, for instance, mechanotransduction of shear stress [53–55], exclusion of red blood cells [56–59], and modulation of the attachment and rolling of leukocyte [52, 60, 61]. However, the tribological role of the glycocalyx is poorly investigated. We first studied the role of glycocalyx on sliding friction of living HUVEC monolayer and found that glycocalyx may play a vital role in reducing the surface friction of endothelial cell monolayer [53].

Actually, it is difficult to analyze the tribological properties of the cells cultured on the surface of hard and dry substrates (e.g., cover glasses and TCPS), because the cells are easily destroyed due to stress concentration. The soft and viscoelastic hydrogel, facilitating cell proliferation, is the optimum material for relieving the stress concentration. We solved the problem by proposing a strategy of establishment of a system of testing surface friction of living cells, in which the endothelial cell monolayers are cultured on soft PNaSS hydrogel ($M = 10$ mol%, $E = 59.4$ kPa). The system of testing frictional behaviors of living cells consists of HUVEC monolayer cultured on PNaSS hydrogel and an opposing substrate (glass, hydrogel, or any preferred material). The detailed test processes based on rheometer are as follows. A disk-shaped hydrogel (diameter is 7.5 mm) with a HUVEC monolayer on one

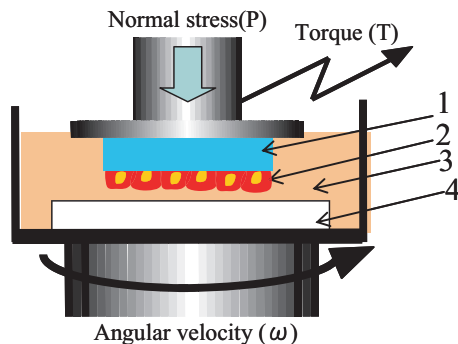


Fig. 2.17 Schematic representation of the experimental setup for friction measurement of the HUVEC monolayers cultured on PNaSS hydrogel: (1) disk-shaped hydrogel, (2) HUVEC monolayer cultured on the hydrogel, (3) protein-free cell culture medium, and (4) opposing substrate (i.e., glass plate or HUVEC monolayer cultured on PNaSS hydrogel). (Reprinted with permission from Ref. [53], Copyright 2010 Wiley)

surface was used as the test sample. The bare surface of the hydrogel is glued onto the upper surface of a coaxial disk platen; an opposing substrate, flat glass (30 mm × 30 mm), or a disk-shaped PNaSS hydrogel (12.5 mm diameter) loading a HUVEC monolayer is glued onto the bottom of the container (120 mm diameter), serving as opposing sliding substrate, paralleling to the upper platen. The test sample and opposing substrate are compressed and contact with each other under a normal pressure (P) of 3.3 kPa in protein-free Humedia-EB2 medium (HEM) (37 °C) (Fig. 2.17). The torque ($T(\omega)$) can be detected when the opposing sliding substrate rotates with an angular velocity (ω) at a strain-constant mode. The maximum sliding velocity ($\nu = \omega R$) at the edge of the disk-shaped hydrogel is in the range of $7.5 \times 10^{-6} - 7.5 \times 10^{-5}$ m/s when $\omega = 10^{-3} - 10^{-2}$ rad/s. Since the sliding velocity changes with the distance from the center of the axis, the obtained torque, $T(\omega)$, is an integrated value all over the plate [62]. Frictional stress (frictional force per unit area) between the cell monolayer and sliding substrate corresponding to the sliding velocity of ωR is $\sigma(\omega R) = [(3 + \alpha)T(\omega)]/(2 + \alpha)\pi R^3$, supposing that the torque has a power relation with ω as $T(\omega) \approx \omega^\alpha (\alpha = 0-1)$. Therefore, frictional stress can be calculated as $\sigma(\omega R) = [4T(\omega)]/3\pi R^3$ when $\alpha = 1$.

We verified the role of glycocalyx on friction reduction of HUVEC monolayer through modulating the amount of glycocalyx, by treating the as-cultured HUVEC monolayers with TGF- β_1 and heparinase I. The glycosaminoglycan chains of HSPGs can be elongated by TGF- β_1 treatment [50], leading to thickness enhancement, but cleaved by heparinase I, leading to thickness reduction [63]. According to immunostaining analysis, the increased fluorescence intensity of HSPGs on the cultured HUVEC monolayer is 148% due to TGF- β_1 treatment and 57.0% decrease by heparinase disruption.

In order to accurately measure the surface friction of the HUVEC monolayers, we need to identify the suitable testing conditions under which most HUVECs remain adherent and live on the hydrogel surface in the process of friction test.

Actually, HUVECs are easily detached from hydrogel surface, especially at a high sliding velocity. When the sliding velocity was increased to 7.5×10^{-4} m/s, the HUVECs were detached from the surface of hydrogel in a few seconds before the frictional stress became constant. We identified the time that more than 80% HUVECs adhere to the hydrogel surface ($T_{80\%}$) for the as-cultured, TGF- β_1 -treated, and heparinase I-treated HUVEC monolayer, sliding with flat glass or identical cell monolayers (Fig. 2.17). The $T_{80\%}$ under different sliding velocities of as-cultured and TGF- β_1 -treated cell monolayers is similar. The values of $T_{80\%}$ are as high as ~ 1400 s and ~ 1800 s when the cell monolayers slide against flat glass or identical cell monolayers, respectively, and when sliding velocity is 7.5×10^{-6} m/s. The values decline to ~ 1200 s and ~ 600 s when sliding velocity is increased to 2.75×10^{-5} m/s, whereas the values sharply decrease for the heparinase I-treated samples, especially when the sliding velocity is larger than 2.37×10^{-5} m/s. The $T_{80\%}$ of all HUVEC samples rapidly decreased to less than 100 s when the sliding velocity is increased to 7.5×10^{-5} m/s, regardless of TGF- β_1 or heparinase I treatment. The higher frictional stress and strength reduction of endothelial cell adhesion on the template may lead to the phenomenon [39]. After testing, the test sample was collected, and the cells that remain on the hydrogel surface were cultured in incubator again. We found that the cells adhered on hydrogel can expand on the hydrogel surface after the testing of friction behaviors. The aforementioned results identify a suitable testing conditions, that is, most cells remain living on the hydrogel surface in the process of friction test.

To compare the friction behaviors of as-cultured, TGF- β_1 -treated and heparinase I-treated HUVEC monolayers, the following frictions between cell monolayers and flat glass or identical cell monolayers were performed. There are three sets of cell monolayer glass/cell monolayer samples, i.e., (1) as-cultured HUVEC monolayer vs. glass/as-cultured HUVEC monolayers, (2) TGF- β_1 -treated HUVEC monolayer vs. glass/TGF- β_1 -treated HUVEC monolayer, and (3) heparinase I-treated HUVEC monolayer vs. glass/heparinase I-treated HUVEC monolayer. The typical time profiles of the frictional stresses of as-cultured, TGF- β_1 -treated, and heparinase I-treated HUVEC monolayers sliding against flat glass substrate at a sliding velocity of 7.5×10^{-6} m/s are shown in Fig. 2.18.

The three samples show similar time profiles; frictional stresses of HUVEC monolayers rapidly increase initially and reach a peak at a few seconds (the peak value is adopted as static friction stress, σ_{stat}). Then, the values gradually decrease with sliding time and became constant after several tens of seconds (the constant value is adopted as dynamic frictional stress, σ_{dyn}). The static (μ_{stat}) and dynamic (μ_{dyn}) friction coefficient can be calculated as the ratio of σ_{stat} (σ_{dyn}) to the applied normal stress. The frictional behavior is remarkably affected by glycocalyx treatment. The static (σ_{stat} , μ_{stat}) and dynamic (σ_{dyn} , μ_{dyn}) frictional stress and frictional coefficient for the as-cultured, TGF- β_1 -treated, and heparinase I-treated samples with various amount of glycocalyx are summarized in Fig. 2.19. The σ_{stat} and σ_{dyn} frictional stress of HUVEC monolayer decrease in the following order: heparinase I-treated > as-cultured > TGF- β_1 -treated samples. The mechanism can be understood as follows. Glycocalyx can be considered as a hydrogel layer with negative

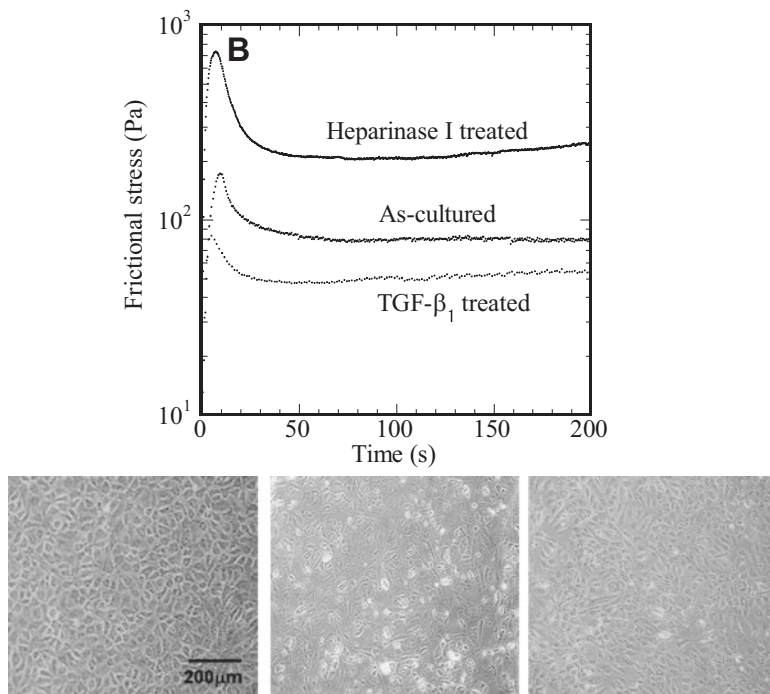


Fig. 2.18 The time profiles of frictional stress of the as-cultured, TGF- β_1 -treated, and heparinase I-treated HUVEC monolayers (upper). Sliding substrate: flat glass, sliding velocity: $7.5 \times 10^{-6} \text{ m s}^{-1}$. The morphology of as-cultured (lower, left), heparinase I-treated (lower, middle), and TGF- β_1 -treated (lower, right) HUVEC monolayers. (Reprinted with permission from Ref. [53], Copyright 2010 Wiley)

charges. Theoretically, it contains 1 ~ 2% negatively charged acidic glycosaminoglycan side chains with many carboxyl and sulfate groups [64, 65]. On the other hand, the SiOH groups on the surface of glass are negatively charged at pH = 7.4. Thus, there is osmotic repulsion formed in the interface of two like-charged sliding surfaces, when negatively charged monolayer of endothelial cells slides against flat glass or identical cell monolayer in aqueous solution. Thus, a lubricating water layer at the interface sustained by dissociating counterions of cell monolayer and sliding substrate contributes to lubrication. Accordingly, the effect of glycocalyx on the reduction of cell friction can be understood as follows. After TGF- β_1 treatment, the amount of glycocalyx is enhanced, favoring water holding and formation of hydration layer, leading to lubrication and friction reduction. On the other hand, after heparinase I treatment, the amount of glycocalyx is declined due to poor hydration and water holding, leading to high friction. Moreover, the loose cell-cell contact and the change of cell morphology which are derived from heparinase I treatment may also influence the sliding properties.

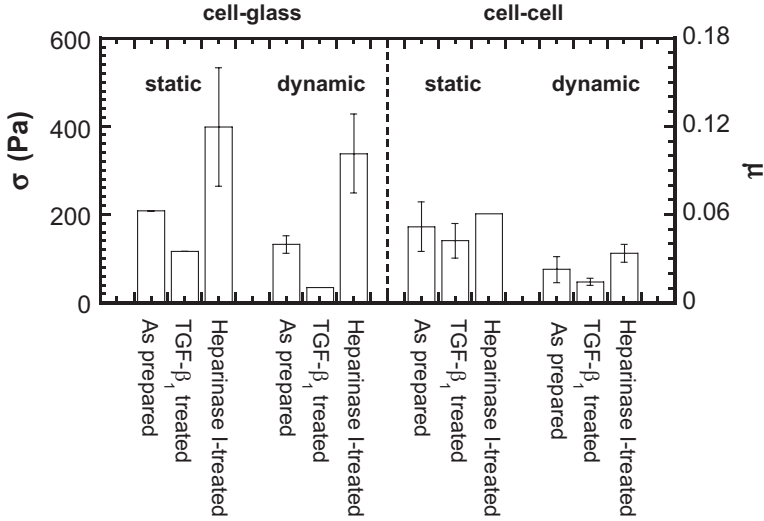


Fig. 2.19 The static (σ_{stat}) and dynamic (σ_{dyn}) frictional stress of HUVEC monolayer vs. glass/identical cell monolayers, for as-cultured, heparinase I-treated, and TGF- β_1 -treated samples. The right vertical axis is the corresponding results of static (μ_{stat}) and dynamic (μ_{dyn}) frictional coefficient. Sliding velocity: 7.5×10^{-6} m/s. (Reprinted with permission from Ref. [53], Copyright 2010 Wiley)

The developed approach for testing surface friction of living endothelial cells using a rheometer has the following advantages:

1. No limitation of the type of endothelial cells. It is even possible to evaluate the friction behaviors of living human endothelial cells cultured on hydrogel templates, but is not limited by real tissue samples.
2. No limitation of the type of sliding materials. It is possible to evaluate the friction behaviors between endothelial cell monolayers and various biomaterials for clinic, for instance, metals, ceramics, and elastomers, in cell culture medium.
3. The high sensitivity in detecting extremely small frictional stress and coefficient.

2.6.3 Selective Cell Adhesion and Proliferation on Micro-Patterned Hydrogel Surfaces

Cultivation of cells on micro-patterned templates is important to understand the cell behaviors in complex tissues where available geometric space is limited, such as in the branching networks of capillary vessels [66, 67]. It has been reported that the topographical patterns of templates remarkably affect cell growth, morphology,

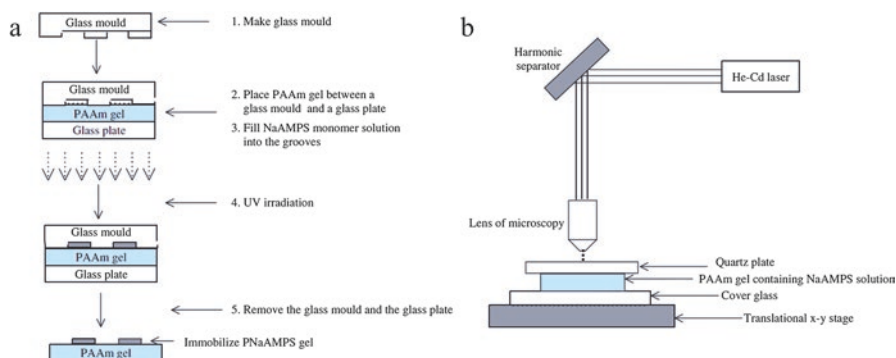


Fig. 2.20 Schematic representations of fabricating micro-patterned PNaAMPS hydrogel on the surface of PAAm hydrogel substrate. **(a)** Glass mold transfer method. **(b)** Laser beam polymerization method. (Reprinted with permission from Ref. [69], Copyright 2007 American Scientific Publishers)

viability, and gene expression [68]. As aforementioned, we have found that negatively charged hydrogels, such as PNaAMPS and PNaSS, facilitate endothelial cell spread and proliferate to monolayer, under the condition which requires no surface modification of any cell-adhesive proteins or peptides. However, neutral hydrogels, such as PAAm, strongly inhibited cell expansion. On the base of these, we can design and fabricate micro-patterned hydrogel surfaces. The stable micro-patterns of PNaAMPS hydrogel can be fabricated on the substrate of PAAm hydrogel (micro-patterned PNaAMPS/PAAm hydrogel), by the approaches of a two-step sequential network formation, i.e., glass mold transfer and laser beam polymerization [69]. The processes of glass mold transfer are as follows. Firstly, a glass mold with grooves on its surface is made by a diamond point, then sandwiching a piece of as-prepared PAAm ($M = 4$ mol%) hydrogel ($100 \times 100 \times 2$ mm) between the glass mold and a plate of flat glass, and then subsequently filling the precursor solution of PNaAMPS hydrogel (1 M NaAMPS, 4 mol% MBAA, 0.1 mol% 2-oxoglutaric acid) into the grooves by capillary effect. After polymerization under UV light, a piece of hydrogel with PNaAMPS micro-patterns can be obtained (Fig. 2.20a). An advanced laser processing system is used for the approach of laser beam polymerization, and the processes are as follows. Firstly, the PAAm substrate ($18 \times 18 \times 2$ mm) is prepared by equilibrating pieces of as-prepared PAAm hydrogel into the precursor solution of PNaAMPS hydrogel. The hydrogel mold is put onto a cover glass loading onto a stage which can be precisely 3D operated under computer control. After sheltering by a quartz plate, a beam of He-Cd laser (325 nm, 15.3 mW) focuses on the PAAm substrate through an objective lens for fabricating the micro-patterns of PNaAMPS hydrogel. The ALPS 3220 program supported the pattern design (parallel lines or curves), and laser trajectories (the speed of laser scanning is in the range of $20\text{--}50 \mu\text{m s}^{-1}$) are used for polymerization (Fig. 2.20b).

The micro-patterned PNaAMPS/PAAm hydrogel with a straight stripe with large size ($182 \mu\text{m}$ width) can be fabricated by the approach of glass mold transfer

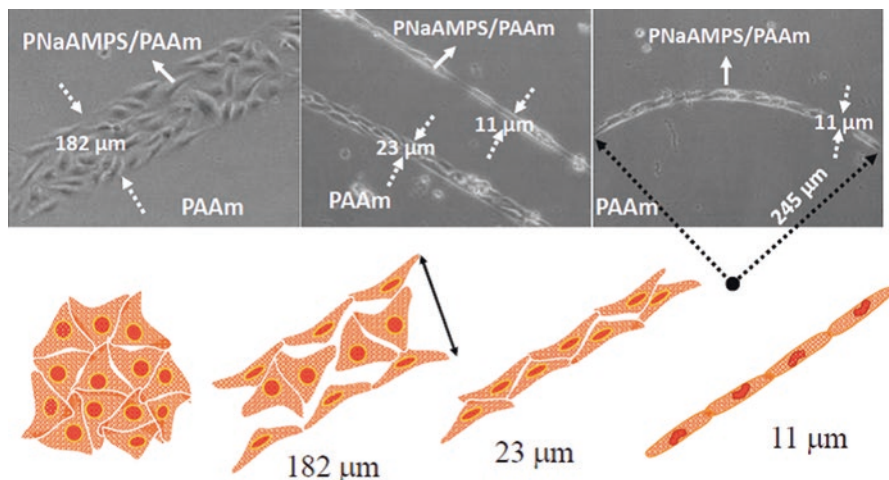


Fig. 2.21 Phase-contrast micrographs and schematic representations of BFAECs cultured on the surfaces of PNaAMPS/PAAm micro-patterned hydrogels. (a) The straight stripe with 182- μm width. (b) The straight stripe with 11- μm (upper) and 23- μm (lower) width. (c) Curved stripe with 11- μm width and 245- μm radius. Scale bar 100 μm . (Reprinted with permission from Ref. [69], Copyright 2007 American Scientific Publishers)

(Fig. 2.20a), due to the size limitation of diamond point. It is difficult to fabricate the micro-patterns with the width less than 200 μm . The micro-patterned hydrogels with straight stripes (11 μm and 23 μm width) and curved stripes (11 μm width, the radius of the curve is 245 μm) can be fabricated by the approach of laser beam polymerization (Fig. 2.20b). Laser beam polymerization method is more suitable for fabricating the PNaAMPS/PAAm pattern with small size. After seeding BFAECs (2.26×10^4 cells/ cm^2 in density) onto the surface of micro-patterned PNaAMPS/PAAm hydrogels, it is clear that the cells selectively adhere and homogeneously distribute on the straight or curved PNaAMPS stripes. The cell behaviors obviously depend on the size of micro-patterns. On the 182- μm straight stripe, cells on the straight stripe can proliferate to confluence with 96 h, which is similar to that on the bulk PNaAMPS hydrogel (Fig. 2.21a). Because the width of the stripe is much larger than the size of cells (~ 50 μm), it does not remarkably influence the orientation of all cells. There are two kinds of orientation of the cells, i.e., stripe parallel and randomness. Only the cells living on the verge of stripe show an identical orientation along the stripe. The number of cells lining along the stripe verge increases with culture time, whereas the cells living on the middle of stripe show almost random orientation and polygonal shape. With the reduction of stripe width, the cells spread well in a fusiform shape with enhanced orientation and align along the stripe more compactly. On the 23- μm straight stripes, cells can proliferate to confluence for 24 h, and more than 90% of the cells show the identical orientation along the verge of stripe (Fig. 2.21b). When the width of stripe is further declined to 11 μm , for both straight and curved stripes, the cells reach confluence at 6 h, and all the cells are

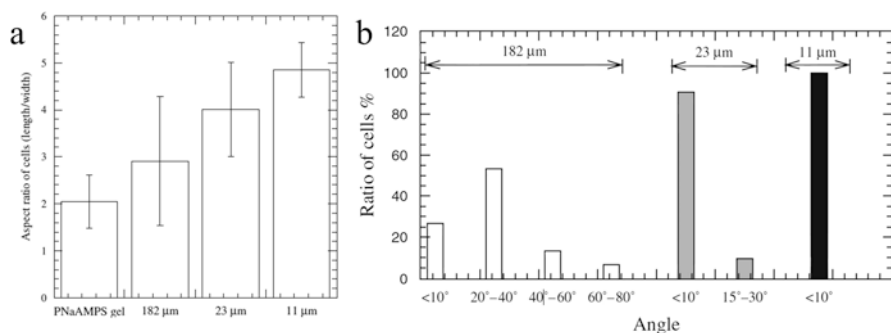


Fig. 2.22 (a) Aspect ratio of the length of the longest axis to the width of cells cultured on different scaffolds when cells proliferate to confluence. (b) Ratio of cells as a function of the angles between the stripe verge of the micro-patterns and the longest axis of the cells on different scaffolds when cells were cultured at 24 h. (Reprinted with permission from Ref. [69], Copyright 2007 American Scientific Publishers)

lined along the verges of stripes and curves with a fusiform shape hand in hand (Fig. 2.21b, c).

For quantitative characterization of cell morphology and arrangement, the cell behaviors of anisotropic spreading and angle of cell alignment are further analyzed (Fig. 2.22). The anisotropic spreading is represented by aspect ratio of the length of the longest axis to the width of cells. The large value reveals the high degree of anisotropic spreading of cells. The aspect ratio increases with a decline of the width of micro-patterned PNaAMPS/PAAm stripes. The average aspect ratio of cells cultured on micro-patterned 23- and 11 μm -wide stripes is 4.01 ± 1.0 and 4.85 ± 0.58 , respectively, which is obviously larger than that of the cells cultured on 182- μm -wide stripe (2.91 ± 1.37) and bulk PNaAMPS hydrogel (2.05 ± 0.56). The angle of cell alignment is the angle between the stripe verge of micro-patterns and the longest axis of cells. The small angle represents high alignment of cell along the stripes. The cells with the angle lower than 10° are considered as aligning along the patterns. Similar with the aspect ratio, the angle of cell alignment increases with the decrease of the width of micro-patterned stripes. For 11- μm -wide stripes, 100% cells exhibit the angle lower than 10° , demonstrating that all cells arrange along the stripes. When the width of the stripe is increased to 23 μm , ~90% cells exhibit the angle lower than 10° , and ~10% cells exhibit the angle in a range of 15–30°. Further increasing the width to 182 μm , only ~27% cells show the angle lower than 10° , ~55% cells appear the angles in a range of 20–40°, and other cells emerge the high angle (40–80°). The results demonstrated that the geometric limitation of hydrogel can modulate cell shape and direction. The morphology of cells changes from a polygonal to a fusiform shape, and cells uniformly orient in the direction of the long axis of micro-patterned stripes, when the width of stripe is smaller than the size of cells.

2.6.4 Tough Hydrogels for Cell Adhesion and Proliferation

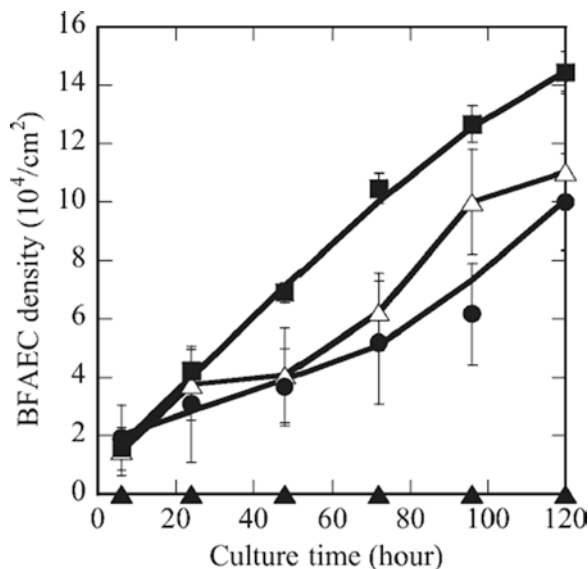
Mechanical properties are critically vital when using hydrogels in tissue engineering. Many tissues including cartilages, tendons, ligaments, and blood vessels bear severe force in physiological condition. However, the mechanical weakness of traditional hydrogels confines them to limited low-level loading areas, for instance, drug delivery systems, hyperthermia cancer therapy, and enzyme immobilization. The tough hydrogels with superior mechanical properties are expected to lead to breakthrough applications, such as the prosthetic materials for soft tissues, where some critical parameters, toughness and cellular viability, are two prior parameters. The hydrogels with both cell compatibility and high mechanical strength will substantially promote the application of tough hydrogels in biomedical field.

To meet this demand, we developed tough triple network (TN) hydrogels, which preserve high mechanical strength and, at the same time, facilitate cell proliferation. The TN PNaAMPS/PDMAAm/poly(NaAMPS-co-DMAAm) hydrogels can be synthesized by the introduction of the triple copolymer networks of poly(NaAMPS-PDMAAm) to PNaAMPS/PDMAAm double-network (DN) hydrogels. The reported typical DN hydrogels, such as PNaAMPS/PDMAAm and PNaAMPS/PAAm, which have fracture strength as high as few tens MPa, do not facilitate cell proliferation, because the surface of the DN hydrogels is covered by a layer of neutral polymer networks. In the process of DN synthesis, the second network derived from neutral monomers, including DMAAm and AAm, prefers to polymerize on the surface of the first network, PNaAMPS. That is, the surface properties of DN hydrogels are dominated by the second networks of neutral components. This is confirmed by the adsorptive interaction between the neutral hydrogels and glass substrate, for instance, the force interaction tested by atomic force microscopy (AFM) and high frictional coefficient ($\sim 10^{-1}$) measured by a rheometer [70].

In fact, there is a contradiction in the design of tough TN hydrogels with cell compatibility. Negatively charged polymers, PNaAMPS, facilitate cell proliferation but decrease mechanical property, while neutral polymers, e.g., PDMAAm and PAAm, enhance mechanical property but lack cell proliferation. In order to design TN hydrogels with dual functions of cell proliferation and toughness, we should balance the molar ratio of PNaAMPS and PDMAAm or PAAm. Based on the previously described effect of critical charge on cell behaviors, we designed the tough TN hydrogels that facilitate cell spreading and proliferation and, at the same time, preserve high mechanical strength, by inducing copolymer networks as the third component to DN hydrogels.

The poly(NaAMPS-co-PDMAAm) ($F = 0.5$, $M = 4$ mol%) was chosen as the polymer of triple networks. Its zeta potential is as low as -22.0 mV, facilitating protein adsorption and further cell proliferation. As expected, when the cross-linking concentrations of the poly(NaAMPS-co-DMAAm) are 2 and 4 mol% (TN-2, TN-4), the TN hydrogels exhibit ~ 2 MPa compressive strength, obviously higher than that of single-network hydrogel, PNaAMPS (0.63 MPa), and poly(NaAMPS-

Fig. 2.23 The densities of BFAECs cultured on the TN hydrogels with different cross-linking concentration of the third network, poly(NaAMPS-co-DMAAm) ($M = 4$ mol %) as a function of culture time. (\blacktriangle): 0 mol %, (\bullet): 2 mol %, and (\triangle): 4 mol %. (\blacksquare) poly(NaAMPS-co-DMAAm) $F = 0.5$ ($M = 4$ mol %). (Reprinted with permission from Ref. [16], Copyright 2009 Wiley)



co-DMAAm) (0.26 MPa). At the same time, the TN hydrogels can promote BFAEC proliferation to a monolayer with the cell density of 1×10^5 cell/cm² at 120 h. The results indicate that the poly(NaAMPS-co-PDMAAm) networks decorated on the surface of the TN hydrogels determine cell behaviors. However, when the poly(NaAMPS-co-DMAAm) is not cross-linked (TN-0), although the compressive strength is as high as 3.0 MPa, the cells cannot proliferate. The high mobility of the linear polymer chains on the surface of TN-0 hydrogel may not facilitate cell spreading and proliferation.

Notably, the cell density and proliferation ratio of TN-2 and TN-4 hydrogels are lower than that of poly(NaAMPS-co-DMAAm) hydrogel (Fig. 2.23). The Young's modulus and zeta potential of the hydrogels may be responsible for the difference. According to our previous results, the rate of BFAEC proliferation increases with Young's modulus when it is in a range of 1–10 kPa. When the Young's modulus is higher than 10 kPa, the cell density and proliferation rate are not obviously dependent on the stiffness. The Young's modulus of the TN hydrogels (650 kPa for TN-2, 880 kPa for TN-4) is obviously higher than 10 kPa; thus, it does not affect cell behaviors. According to above consideration, a slightly high charge density of the copolymer hydrogel than that of the TN hydrogels may lead to the phenomena of low cell density and slow cell proliferation. The TN hydrogels are thermal and chemically stable, and after cell cultivation or even sterilization under higher temperature (120 °C), their mechanical strength is maintained. The tough and cell-proliferated TN hydrogel will substantially promote the application of tough hydrogels as soft and wet tissues, such as hybrid artificial blood vessel with inner endothelial cell monolayer.

2.7 Conclusions

We have established a cell culture system based on protein-free synthetic hydrogels, presenting many opportunities of the soft and wet biomaterial served as active templates for controlling the behaviors and functions of in vitro cultured cells. The negatively charged synthetic hydrogels without modification by any cell-adhesive proteins or peptides, including PNaSS, PNaAMPS, PAA, and PMAA, can promote cell adhesion and proliferation under the environment of serum-containing medium. We found that so long as the zeta potential of synthetic hydrogels is lower than ca. -20 mV, they can facilitate the adhesion and proliferation of endothelial cells. On the basis of this unique cell culture system, we can systematically investigate the effect of physicochemical properties of fully synthetic hydrogels on cell behaviors and functions. The results demonstrate that the chemical structure, charge density, and surface topography of synthetic hydrogels affect static cell behaviors (adhesion, spreading, morphology, proliferation, cytoskeletal structure, and focal adhesion), dynamic cell behaviors (migration velocity, morphology oscillation), and cell functions (platelet compatibility, surface friction). The concept of tuning cell behaviors by synthetic hydrogels may be broadly applicable to design and choose suitable polymer biomaterials for the applications of tissue engineering. We propose that as an ideal biomaterial for tissue engineering, it should not only favor cell proliferation but also keep the original functions of the in vitro cultured cells.

References

1. Chen YM, Ogawa R, Kakugo A et al (2009) Dynamic cell behavior on synthetic hydrogels with different charge densities. *Soft Matter* 5:1804–1811
2. Nguyen KT, West JL (2002) Photopolymerizable hydrogels for tissue engineering applications. *Biomaterials* 23:4307–4314
3. Georges PC, Janmey PA (2005) Cell type-specific response to growth on soft materials. *J Appl Physiol* 98:1547–1553
4. Liu JF, Chen YM, Yang JJ et al (2011) Dynamic behavior and spontaneous differentiation of mouse embryoid bodies on hydrogel substrates of different surface charge and chemical structures. *Tissue Eng Part A* 17:2343–2357
5. Kleinman HK, Martin GR (2005) Matrigel: basement membrane matrix with biological activity. *Semin Cancer Biol* 15:378–386
6. Bessea L, Coulomb B, Lebreton-Decoster C et al (2002) Production of ordered collagen matrices for three-dimensional cell culture. *Biomaterials* 23:27–36
7. Szot CS, Buchanan CF, Freeman JW et al (2011) 3D in vitro bioengineered tumors based on collagen I hydrogels. *Biomaterials* 32:7905–7912
8. Willerth SM, Arendas KJ, Gottlieb DI et al (2006) Optimization of fibrin scaffolds for differentiation of murine embryonic stem cells into neural lineage cells. *Biomaterials* 27:5990–6003
9. Geckil H, Xu F, Zhang XH et al (2010) Engineering hydrogels as extracellular matrix mimics. *Nanomedicine (Lond)* 5:469–484
10. Yang F, Williams CG, Wang DA et al (2005) The effect of incorporating RGD adhesive peptide in polyethylene glycol diacrylate hydrogel on osteogenesis of bone marrow stromal cells. *Biomaterials* 26:5991–5998

11. Tibbitt MW, Anseth KS (2009) Hydrogels as extracellular matrix mimics for 3D cell culture. *Biotechnol Bioeng* 103:655–663
12. Azagarsamy MA, Anseth KS (2013) Bioorthogonal click chemistry: an indispensable tool to create multifaceted cell culture scaffolds. *ACS Macro Lett* 2:5–9
13. Liu ZQ, Wei Z, Zhu XL et al (2015) Dextran-based hydrogel formed by thiol-Michael addition reaction for 3D cell encapsulation. *Colloids Surf B Biointerfaces* 128:140–148
14. Chen YM, Shiraiishi N, Satokawa H et al (2005) Cultivation of endothelial cells on adhesive protein-free synthetic polymer gels. *Biomaterials* 26:4588–4596
15. Chen YM, Liu ZQ, Feng ZH et al (2014) Adhesive protein-free synthetic hydrogels for retinal pigment epithelium cell culture with low ROS level. *J Biomed Mater Res A* 102:2258–2267
16. Chen YM, Gong JP, Tanaka M et al (2009) Tuning of cell proliferation on tough gels by critical charge effect. *J Biomed Mater Res A* 88:74–83
17. Chen YM, Tanaka M, Gong JP et al (2007) Platelet adhesion to human umbilical vein endothelial cells cultured on anionic hydrogel scaffolds. *Biomaterials* 28:1752–1760
18. Chen YM, Dong K, Liu ZQ et al (2012) Double network hydrogel with high mechanical strength: performance, progress and future perspective. *Sci China Technol Sci* 55:2241–2254
19. Yang JJ, Chen YM, Liu JF et al (2010) Spontaneous redifferentiation of dedifferentiated human articular chondrocytes on hydrogel surfaces. *Tissue Eng Part A* 16:2529–2540
20. Kwon HJ, Yasuda K, Ohmiya Y et al (2010) In vitro differentiation of chondrogenic ATDC5 cells is enhanced by culturing on synthetic hydrogels with various charge densities. *Acta Biomater* 6:494–501
21. Maroudas NG (1975) Adhesion and spreading of cells on charged surfaces. *J Theor Biol* 49:417–424
22. Schneider GB, English A, Abraham M et al (2004) The effect of hydrogel charge density on cell attachment. *Biomaterials* 25:3023–3028
23. Narita T, Hirai A, Xu J et al (2000) Substrate effects of gel surfaces on cell adhesion and disruption. *Biomacromolecules* 1:162–167
24. Magnani A, Priamo A, Pasqui D et al (2003) Cell behaviour on chemically microstructured surfaces. *Mater Sci Eng C* 23:315–328
25. Nakayama Y, Anderson JM, Matsuda T (2000) Laboratory-scale mass production of a multi-micropatterned grafted surface with different polymer regions. *J Biomed Mater Res* 53:584–591
26. Lee JH, Lee JW, Khang G et al (1997) Interaction of cells on chargeable functional group gradient surfaces. *Biomaterials* 18:351–358
27. Sugimoto Y (1981) Effect on the adhesion and locomotion of mouse fibroblasts by their interacting with differently charged substrates: a quantitative study by ultrastructural method. *Exp Cell Res* 135:39–45
28. Lee J, Ko M, Joo CK (2008) Rho plays a key role in TGF-beta1-induced cytoskeletal rearrangement in human retinal pigment epithelium. *J Cell Physiol* 216:520–526
29. Bronnerfraser M (1993) Neural crest cell migration in the developing embryo. *Trends Cell Biol* 3:392–397
30. Singer SJ, Kupfer A (1986) The directed migration of eukaryotic cells. *Annu Rev Cell Biol* 2:337–365
31. Hauzenberger D, Klominek J, Holgersson J et al (1997) Triggering of motile behavior in T lymphocytes via cross-linking of alpha 4 beta 1 and alpha L beta 2. *J Immunol* 158:76–84
32. McCawley LJ, O'Brien P, Hudson LG (1997) Overexpression of the epidermal growth factor receptor contributes to enhanced ligand-mediated motility in keratinocyte cell lines. *Endocrinology* 138:121–127
33. Van Roy F, Mareel M (1992) Tumour invasion: effects of cell adhesion and motility. *Trends Cell Biol* 2:163–169
34. Lamalice L, Le Boeuf F, Huot J (2007) Endothelial cell migration during angiogenesis. *Circ Res* 100:782–794
35. Davis GE, Senger DR (2005) Endothelial extracellular matrix: biosynthesis, remodeling, and functions during vascular morphogenesis and neovessel stabilization. *Circ Res* 97:1093–1107

36. Moon JJ, Matsumoto M, Patel S et al (2005) Role of cell surface heparan sulfate proteoglycans in endothelial cell migration and mechanotransduction. *J Cell Physiol* 203:166–176
37. van den Berg BM, Vink H, Spaan JA (2003) The endothelial glycocalyx protects against myocardial edema. *Circ Res* 92:592–594
38. Calonder C, Matthew HW, Van Tassel PR (2005) Adsorbed layers of oriented fibronectin: a strategy to control cell-surface interactions. *J Biomed Mater Res A* 75:316–323
39. Polte TR, Eichler GS, Wang N et al (2004) Extracellular matrix controls myosin light chain phosphorylation and cell contractility through modulation of cell shape and cytoskeletal pre-stress. *Am J Phys* 286:C518–C528
40. Rowley JA, Madlambayan G, Mooney DJ (1999) Alginate hydrogels as synthetic extracellular matrix materials. *Biomaterials* 20:45–53
41. Belmadani S, Zerfaoui M, Boulares HA et al (2008) Microvessel vascular smooth muscle cells contribute to collagen type I deposition through ERK1/2 MAP kinase, α v β 3-integrin, and TGF- β 1 in response to ANG II and high glucose. *Am J Phys* 295:H69–H76
42. Yanagishita M, Hascall VC (1992) Cell surface heparan sulfate proteoglycans. *J Biol Chem* 267:9451–9454
43. Hallgren J, Spillmann D, Pejler G (2001) Structural requirements and mechanism for heparin-induced activation of a recombinant mouse mast cell tryptase, mouse mast cell protease-6: formation of active tryptase monomers in the presence of low molecular weight heparin. *J Biol Chem* 276:42774–42781
44. Woods AM, Rodenberg EJ, Hiles MC et al (2004) Improved biocompatibility of small intestinal submucosa (SIS) following conditioning by human endothelial cells. *Biomaterials* 25:515–525
45. Nugent MA, Nugent HM, Iozzo RV et al (2000) Perlecan is required to inhibit thrombosis after deep vascular injury and contributes to endothelial cell-mediated inhibition of intimal hyperplasia. *Proc Natl Acad Sci USA* 97:6722–6727
46. Segev A, Nili N, Strauss BH (2004) The role of perlecan in arterial injury and angiogenesis. *Cardiovasc Res* 63:603–610
47. Guyton JR, Rosenberg RD, Clowes AW et al (1980) Inhibition of rat arterial smooth muscle cell proliferation by heparin. In vivo studies with anticoagulant and nonanticoagulant heparin. *Circ Res* 46:625–634
48. Kaji T, Yamada A, Miyajima S et al (2000) Cell density-dependent regulation of proteoglycan synthesis by transforming growth factor- β (1) in cultured bovine aortic endothelial cells. *J Biol Chem* 275:1463–1470
49. Kasinath BS (1993) Glomerular endothelial-cell proteoglycans – regulation by Tgf- β -1. *Arch Biochem Biophys* 305:370–377
50. Linhardt RJ, Turnbull JE, Wang HM et al (1990) Examination of the substrate specificity of heparin and heparan sulfate lyases. *Biochemistry* 29:2611–2617
51. Florian JA, Kosky JR, Ainslie K et al (2003) Heparan sulfate proteoglycan is a mechanosensor on endothelial cells. *Circ Res* 93:E136–E142
52. Mulivor AW, Lipowsky HH (2002) Role of glycocalyx in leukocyte-endothelial cell adhesion. *Am J Phys* 283:H1282–H1291
53. Chen YM, Kurokawa T, Tominaga T et al (2010) Study on the sliding friction of endothelial cells cultured on hydrogel and the role of Glycocalyx on friction reduction. *Adv Eng Mater* 12:B628–BB36
54. Tarbell JM, Pahakis MY (2006) Mechanotransduction and the glycocalyx. *J Intern Med* 259:339–350
55. Weinbaum S, Zhang X, Han Y et al (2003) Mechanotransduction and flow across the endothelial glycocalyx. *Proc Natl Acad Sci USA* 100:7988–7995
56. Secomb TW, Hsu R, Pries AR (2001) Motion of red blood cells in a capillary with an endothelial surface layer: effect of flow velocity. *Am J Phys* 281:H629–H636
57. Damiano ER (1998) The effect of the endothelial-cell glycocalyx on the motion of red blood cells through capillaries. *Microvasc Res* 55:77–91
58. Feng J, Weinbaum S (2000) Lubrication theory in highly compressible porous media: the mechanics of skiing, from red cells to humans. *J Fluid Mech* 422:281–317

59. Vink H, Duling BR (1996) Identification of distinct luminal domains for macromolecules, erythrocytes, and leukocytes within mammalian capillaries. *Circ Res* 79:581–589
60. Constantinescu AA, Vink H, Spaan JAE (2003) Endothelial cell glycocalyx modulates immobilization of leukocytes at the endothelial surface. *Arterioscler Thromb Vasc Biol* 23:1541–1547
61. Zhang X, Curry FR, Weinbaum S (2006) Mechanism of osmotic flow in a periodic fiber array. *Am J Phys* 290:H844–H852
62. Gong JP, Kagata G, Osada Y (1999) Friction of gels. 4. Friction on charged gels. *J Phys Chem B* 103:6007–6014
63. Pries AR, Secomb TW, Jacobs H et al (1997) Microvascular blood flow resistance: role of endothelial surface layer. *Am J Phys* 273:H2272–H2279
64. Sabri S, Soler M, Foa C et al (2000) Glycocalyx modulation is a physiological means of regulating cell adhesion. *J Cell Sci* 113:1589–1600
65. Shah G, Dubin PL, Kaplan JI et al (1996) Size-exclusion chromatography of carboxyl-terminated dendrimers as a model for permeation of charged particles into like-charged cavities. *J Colloid Interface Sci* 183:397–407
66. Curtis A, Wilkinson C (1997) Topographical control of cells. *Biomaterials* 18:1573–1583
67. Flemming RG, Murphy CJ, Abrams GA et al (1999) Effects of synthetic micro- and nano-structured surfaces on cell behavior. *Biomaterials* 20:573–588
68. Chou L, Firth JD, Uitto VJ et al (1995) Substratum surface topography alters cell shape and regulates fibronectin mRNA level, mRNA stability, secretion and assembly in human fibroblasts. *J Cell Sci* 108(Pt 4):1563–1573
69. Chen YM, Shen KC, Gong JP et al (2007) Selective cell spreading, proliferation, and orientation on micropatterned gel surfaces. *J Nanosci Nanotechnol* 7:773–779
70. Kurokawa T, Tominaga T, Katsuyama Y, Kuwabara R, Furukawa H, Yoshihito Y, Gong JP (2005). Elastic-hydrodynamic transition of gel friction. *Langmuir* 21:8643–8648